Mitofusins *Mfn1* and *Mfn2* are required in the β-cell to preserve mitochondrial architecture and insulin secretion

Eleni Georgiadou[1], Charanya Muralidharan[2], Michelle Martinez[2], Pauline Chabosseau[1], Alejandra Tomas[1], Fiona Yong Su Wern[3], Theodoros Stylianides[4], Asger Wretlind[5], Cristina Legido-Quigley[5,6], Nour Alsabeeh[7], Céline Cruciani-Guglielmacci[8], Christophe Magnan[8], Mark Ibberson[9], Isabelle Leclerc[1], Yusuf Ali[3], Amelia K. Linnemann[2], Tristan A. Rodriguez[10] and Guy A. Rutter[1,3*].

[1]Section of Cell Biology and Functional Genomics, Division of Diabetes, Endocrinology and Metabolism, Department of Medicine, Imperial College London, London, W12 0NN, UK
[2]Center for Diabetes and Metabolic Diseases, Indiana University School of Medicine, Indianapolis, IN, 46202, USA
[3]Lee Kong Chian School of Medicine, Nanyang Technological University, 637553, Singapore
[4]Loughborough University, Centre of Innovative and Collaborative Construction Engineering, Leicestershire, LE11 3TU, UK
[5]Systems Medicin, Steno Diabetes Center Copenhagen, 2820, Denmark
[6] Institute of Pharmaceutical Science, Kings College London, London, SE1 9NH, UK
[7] Kuwait University, Department of Physiology, Health Sciences Center, 13110, Kuwait
[8]Université de Paris, BFA, UMR 8251, CNRS, Regulation of Glycemia by Central Nervous System, Paris, 75205, France
[9]Vital-IT Group, SIB Swiss Institute of Bioinformatics, Lausanne, CH-1015,Switzerland
[10]National Heart and Lung Institute, Imperial Centre for Translational and Experimental Medicine, Imperial College London, London, W12 0NN, UK

*Address correspondence to Professor Guy A. Rutter, g.rutter@imperial.ac.uk, +44 20 759 43340

Summary

Mitochondrial glucose metabolism is essential for the initiation of insulin release from pancreatic β-cells. Fusion of mitochondria is supported by mitofusin 1 (MFN1) and mitofusin 2 (MFN2). Whether this process is important for glucose sensing by β-cells is unclear. Here, we generated mice with β-cell-selective, adult-restricted deletion of *Mfn1* and *Mfn2* (β*Mfn1/2*-KO), and explored the impact on insulin secretion and glucose homeostasis. β*Mfn1/2*-KO mice displayed higher glycaemia and a >five-fold decrease in plasma insulin post-intraperitoneal glucose injection. Mitochondrial length, glucose-induced hyperpolarization, ATP synthesis and Ca^{2+} accumulation were significantly reduced in β*Mfn1/2*-KO mouse islets. Ca^{2+} dynamics and mitochondrial membrane potential changes were also suppressed *in vivo*. Defective glucose-stimulated insulin secretion in islets isolated from β*Mfn1/2*-KO mice was nevertheless normalised by the addition of GLP-1 receptor agonists. Mitochondrial fusion and fission cycles are thus essential in the β-cell to maintain normal mitochondrial bioenergetics and glucose sensing both *in vitro* and *in vivo*.

Keywords: Type 2 diabetes, pancreatic β-cell, mitochondrial dysfunction, mitofusins, glucose stimulated insulin secretion, Ca^{2+} dynamics, incretins, GLP-1, GIP, Exendin-4.

Introduction

Mitochondria are often referred to as the powerhouses or, more recently, as the "chief executive organelles" (CEO) of the cell, generating most of the energy required to sustain normal function (Anderson, Jackson et al. 2019). Mitochondria are responsible for NAD and NADH production via the Krebs cycle, oxidative phosphorylation, ATP synthesis, fatty acid oxidation and gluconeogenesis, and mitochondrial DNA (mtDNA) distribution. They also contribute to the regulation of apoptosis and their own turnover via mitophagy (Chandhok, Lazarou et al. 2018).

Mitochondrial oxidative metabolism plays a pivotal role in the response of pancreatic β-cells to stimulation by glucose and other nutrients (Panten and Ishida 1974, Maechler and Wollheim 2001, Rutter, Pullen et al. 2015). Thus, as the blood glucose levels increase in the blood, enhanced glycolytic flux and oxidative metabolism in β-cells lead to an increase in ATP synthesis, initiating a cascade of events which involve the closure of ATP-sensitive K^+ (K_{ATP}) channels (Rorsman and Ashcroft 2018), plasma membrane depolarisation and the influx of Ca^{2+} via voltage-gated Ca^{2+} channels (VDCC). The latter mechanism, along with other, less well defined amplifying signals (Henquin 2000), drive the biphasic release of insulin (Rutter, Pullen et al. 2015).

The possibility that changes in mitochondrial function in these cells may contribute to declining insulin secretion and to type 2 diabetes (T2D) has been the subject of extensive investigation (Supale, Li et al. 2012). Reduced glucose-stimulated insulin secretion (GSIS) in β-cells, alongside altered mitochondrial function, dynamics and morphology, were observed in diabetic models (Del Guerra, Lupi et al. 2005, Mulder and Ling 2009, Rutter GA, Georgiadou E et al. 2020).

Besides synthesizing ATP, mitochondria are also one of the main producers of rative oxygen species (ROS) in the cell, inducing oxidative stress and tissue damage (Szendroedi, Phielix et al. 2012). Mitochondrial dysfunction in type 2 diabetic or obese patients suffering from hyperglycaemia was shown to be directly linked with lowered ATP levels and mitochondrial content as well as the development of insulin resistance (Rovira-Llopis, Banuls et al. 2017). Additionally, mitochondrial DNA (mtDNA) variations in human populations are associated with increased or decreased risk of T2D (van den Ouweland, Maechler et al. 1999), while in animal models, alterations in β-cell mtDNA lead to reduced insulin secretion, hyperglycaemia and β-cell death (Haythorne, Rohm et al. 2019).

The multifaceted roles of mitochondria in the cell are associated with an equally variable morphology. Under normal physiological conditions, these organelles repetitively undergo fusion and fission cycles which are essential for their quality control and adaptation to energetic demands (Wada and Nakatsuka 2016). Thus, highly inter-connected mitochondrial networks allow communication and interchange of contents between mitochondrial compartments, as well as with other organelles such as the ER (Rutter and Rizzuto 2000). These networks exist interchangeably with more fragmented structures, displaying more “classical” mitochondrial morphology, with the balance between the two influenced by external stimuli and metabolic demands (Westermann 2012). In many cell types, including insulinoma-derived INS1 cells, a pro-fused state is often observed during starvation where energy production is required for cytoprotection and resistance to apoptosis. The opposite pertains when cells are exposed to nutrient overload in obesity or T2D (Liesa and Shirihai 2013) which can stimulate mitochondrial fission and uncoupled respiration (Liesa and

Shirihai 2013), but is critical for the elimination of damaged mitochondria by mitophagy (Wai and Langer 2016).

Over the past two decades, considerable light has been shed upon the means through which mitochondrial dynamics are controlled at the molecular level. The mitofusins MFN1 and MFN2, homologues of the *D. melanogaster* fuzzy onions (*fzo*) and mitofusin (*dmfn*) gene products (Hwa, Hiller et al. 2002), are key mediators of outer mitochondrial membrane (OMM) fusion. Whilst optic atrophy protein 1 (OPA1) controls inner mitochondrial membrane (IMM) fusion, dynamin related protein 1 (DRP1) is responsible for mitochondrial fission (Yisang Yoon 2011). Other regulators include FIS1, mitochondrial fission factor (MFF) and MiD49/51 (Serasinghe and Chipuk 2017).

In pancreatic β-cells, defects in mitochondrial structure and the accumulation of damaged or depolarised organelles are associated with the development of diabetes in patients and animal models (Wada and Nakatsuka 2016). Changes in mitochondrial fusion and fission dynamics are observed in the pancreatic β-cell in animal models of diabetes (Higa, Zhou et al. 1999, Supale, Li et al. 2012, Gao, Li et al. 2014), and patients with T2D and obesity exhibit smaller and swollen mitochondria in pancreatic tissue samples (Masini, Martino et al. 2017). The latter changes were suggested to be a consequence of hyperglycaemia (Paltauf-Doburzynska, Malli et al. 2004), implying that mitochondrial dynamics may be master regulators of β-cell function (Yu, Robotham et al. 2006).

The expression of mitochondrial fusion regulators in extra-pancreatic tissues is reportedly altered in diabetes, insulin resistant and obese patients, where *MFN2* levels are lowered in skeletal muscle (Zorzano, Liesa et al. 2009). These changes have been

suggested to result from altered expression of the peroxisome proliferator-activated receptor-gamma coactivator-1 alpha (PGCα) and the oestrogen-related receptor alpha (ERRα) (Bach, Pich et al. 2003, Bach, Naon et al. 2005). These alterations are in turn associated with increases in ROS production and impaired mitochondrial respiration in both skeletal muscle and liver through the JNK pathway (Bach, Pich et al. 2003, Bach, Naon et al. 2005, Schrepfer and Scorrano 2016). Whether these changes are the cause, or the consequence, of impaired mitochondrial dynamics, remains unclear (Quiros, Ramsay et al. 2012, Sebastian, Hernandez-Alvarez et al. 2012, Wang, Ishihara et al. 2015).

Heren, we explore the potential impact of mitochondrial fragmentation in the control of insulin secretion. We show that this manoeuvre exerts profound effects on insulin release, β-cell mass and glucose homeostasis. Fragmentation of mitochondria also disrupts glucose-regulated O_2 consumption, ATP production, intracellular Ca^{2+} dynamics and β-cell-β-cell connectivity. Remarkably, the deficiencies in insulin secretion are largely corrected by incretin hormones, suggesting a possible approach to ameliorating the consequences of mitochondrial fragmentation in some forms of diabetes.

Results

Generation of a conditional β*Mfn1/2*-KO mouse line. Efficient deletion of *Mfn1* and *Mfn2* in the β-cell was achieved in adult mice using the Pdx1-Cre^{ERT2} transgene and tamoxifen injection at 7-8 weeks. Deletion was confirmed by qRT-PCR (Fig.**1A**) and Western (immuno-) blotting (Fig.**1B**) analysis. Relative to *β-actin*, expression of the *Mfn1* and *Mfn2* transcripts in isolated islets from β*Mfn1/2*-KO mice decreased by ~83 and 86% accordingly vs control islets ($p<0.01$,$p<0.0001$;Fig.**1A**), compatible with selective deletion in the β-cell compartment (Elayat, el-Naggar et al. 1995). No differences were detected in the expression of other mitochondrial fission and fusion mediator genes such as *Opa1*, *Drp1* and *Fis1* (Fig.**1A**). Body weight did not differ between groups over the first seven weeks post-tamoxifen injection (Suppl.Fig.**1A**). After this period, the mean body weight of β*Mfn1/2*-KO mice fell significantly below that of control animals, with a 13% weight loss apparent at 21-22 weeks ($p<0.05$; Suppl.Fig.**1A**).

β*Mfn1/2*-KO mice are glucose intolerant with impaired GSIS *in vivo.* To study the effects of mitofusin gene deletion in β-cells on systemic glucose homeostasis and insulin secretion *in vivo,* i.p. injections of 1g/kg body weight glucose (IPGTT) were performed on 14-week old β*Mfn1/2*-KO and WT mice (Fig.**1C**). Glucose challenge revealed impaired glucose tolerance in β*Mfn1/2*-KO mice compared to their control littermates with levels of glucose being higher at most time points following glucose injection (Fig.**2C-D**;$p<0.05$,$p<0.01$). Insulin concentrations were also measured following a 3g/kg body weight glucose i.p. injection (Fig.**2E-F**), with plasma sampled at 0, 5, 15 and 30 min. (Fig.**2G**). Basal glucose levels were modestly, higher in KO mice during all glucose challenges. β*Mfn1/2*-KO mice showed dramatically lower

insulin levels upon glucose challenge vs control animals, indicating a severe insulin secretory deficiency (Fig.**2G-H**,$p<0.05$,$p<0.001$,$p<0.0001$).

Insulin tolerance tests revealed unaltered insulin tolerance (percentage change from baseline) in β*Mfn1/2*-KO mice as compared with WT littermates (Fig.**1I-J**;Suppl.Fig.**1B-C**). Nevertheless, KO mice displayed significantly elevated plasma glucose (Suppl.Fig.**1D)** under both fed and fasted conditions. Additionally, an increase in β-ketones was observed in fasted KO mice (Suppl.Fig.**1E**). These changes were inversely related to plasma insulin levels, which were lower in KO than WT mice under both fed and fasted, conditions (Suppl.Fig.**1F**).

Deletion of *Mfn1/2* alters mitochondrial morphology in β-cells. To assess changes in mitochondrial morphology, the mitochondrial fluorescent probe Mitotracker green was used. Deconvolved confocal images uncovered elongated mitochondria in dissociated WT β-cells (Fig.**2A**). In contrast, the mitochondrial network in KO cells was more fragmented (Fig.**2A;** and inset). Mitochondrial structural changes were quantified revealing that the number of mitochondria per cell was not altered between groups (Fig.**2B**). Mitochondrial elongation, circularity and perimeter, on the other hand, were significantly decreased in β*Mfn1/2*-KO cells, indicative of rounder and smaller organelles (Fig.**2B**;$p<0.0001$). Lastly, mitochondrial structure was evaluated in isolated islets by transmission electron microscopy (TEM). This approach confirmed the presence of more highly fragmented mitochondria in KO mouse islets compared to the WT group (Fig.**2C**). Cristae structure and organisation were also markedly altered in β*Mfn1/2*-KO cells. Thus, classical transverse cristae in WT cells were often

completely absent and replaced instead with a single crista running the length of the mitochondrial section (Fig.**2C**;enlarged panels and schematic representations).

Mitofusins are essential to maintain normal glucose-stimulated Ca^{2+} dynamics, mitochondrial membrane potential and ATP synthesis in β-cells. Increased cytosolic Ca^{2+} is a major trigger of insulin exocytosis in response to high glucose (Rutter, Pullen et al. 2015). In order to determine how β-cell-specific *Mfn1/2* deletion might affect this pathway Ca^{2+} dynamics were investigated by live cell fluorescence microscopy in whole islets using the Ca^{2+} sensitive probe Cal-520. After pre-incubation with 3 mmol/L glucose and subsequent perifusion with 17 mmol/L glucose, KO mouse islets exhibited a significantly lower increase in cytosolic Ca^{2+} concentration ($[Ca^{2+}]_{cyt}$) compared to WT islets (AUC,$p<0.01$;Fig.**3A-B**). The K_{ATP} channel opener diazoxide and a depolarising K^+ concentration (20 mmol/L KCl) were then deployed together to bypass the regulation of these channels by glucose. Under these conditions, cytosolic Ca^{2+} increases were not significantly impaired in KO compared to WT animals (Fig.**3A-B**). Subsequently, Ca^{2+} entry into the mitochondrial matrix was determined since this is likely to be important for the stimulation of oxidative metabolism (McCormack, Halestrap et al. 1990, Georgiadou, Haythorne et al. 2020). Alterations in mitochondrial free Ca^{2+} concentration ($[Ca^{2+}]_{mito}$) were apparent in KO whole islets, where a substantial reduction in the response to 17 mmol/L glucose was observed ($p>0.05$; Fig.**3C-D**). Of note, subsequent hyperpolarisation of the plasma membrane with diazoxide caused the expected lowering of mitochondrial $[Ca^{2+}]_{mito}$ in WT islets (reflecting the decrease in $[Ca^{2+}]_{cyt}$;**Fig.3A**), but was almost without effect on KO islets, suggesting a return to near pre-stimulatory $[Ca^{2+}]_{mito}$ levels at this time point in the absence of MFN1 and MFN2.

Finally, we assessed glucose-induced increases in mitochondrial membrane potential ($\Delta\psi_m$) in dissociated β-cells using tetramethyl rhodamine ethyl ester (TMRE) and found that these were sharply reduced in KO vs WT mouse islets (AUC,$p<0.01$;Fig.**3E-F).** Addition of 2-[2-[4-(trifluoromethoxy)phenyl]hydrazinylidene]-propanedinitrile (FCCP) resulted in a similar collapse in apparent $\Delta\psi_m$ in islets from both genotypes (Fig.**3E**). To assess whether mitochondrial fragmentation may impact glucose-induced increases in mitochondrial ATP synthesis we performed real-time fluorescence imaging using the ATP sensor, Perceval (Tarasov and Rutter 2014). Whereas WT islets responded with a substantial and time-dependent rise in the ATP:ADP ratio in response to a step increase in glucose from 3 mmol/L to 17 mmol/L, β*Mfn1/2*-KO β-cells failed to mount any response to this challenge (AUC,$p< 0.05$; Fig.**3G-H**).

β-cell-β-cell connectivity is impaired by *Mfn1/2* ablation. Intercellular connectivity is required in the islet for a full insulin secretory response to glucose (Johnston, Mitchell et al. 2016, Rutter GA, Georgiadou E et al. 2020). To assess this, individual Ca^{2+} traces recorded from Cal-520-loaded beta-cells in mouse islets (Fig.**3A**) were subjected to correlation (Pearson *r*) analysis to map cell-cell connectivity (Suppl.Fig.**2A**). Following perfusion at 17 mmol/L glucose, β*Mfn1/2*-KO β-cells tended to display an inferior, though not significantly different, coordinated activity than WT cells (Suppl.Fig.**2A**), as assessed by counting the number of coordinated cell pairs (Suppl.Fig.**2C**; 0.94 vs 0.90 for WT vs KO, respectively). By contrast, β-cells displayed highly coordinated Ca^{2+} responses upon addition of 20 mM KCl (the latter stimulating depolarisation and a synchronised Ca^{2+} peak) in KO islets. Similarly, analysis of correlation strength in the same islets revealed significant differences in response to 17 mmol/L glucose between genotypes. In fact, KO islets had weaker mean β-β-cell

coordinated activity ($p<0.05$; Suppl. Fig.**2B, D**; 0.88 vs 0.77 for WT vs KO, respectively), indicating that mitofusins affect the strength of connection rather than the number of coordinated β-cell pairs. Nevertheless, no significant changes were observed in the expression of the gap junction protein *Cx36/Gjd2* between the groups (Suppl.Fig.**2E**).

We also explored β-cell connectivity using signal binarisation to determine whether a hierarchy existed in the degree to which individual β-cells were coupled across the islet (Johnston, Mitchell et al. 2016, Salem, Silva et al. 2019). Clear adherence to a power law distribution of connected β-cells was apparent in the WT islet group in the elevated glucose condition where 5.70% of the β-cells hosted at least 60% of the connections with the rest of the β-cells (R^2=0.15; Suppl.Fig.**3**). Interestingly, no clear adherence to a power-law distribution of connected β-cells was present in the KO group (R^2=0.002) despite displaying a higher percentage (15.06%) of β-β-cell connections.

Unaltered ER Ca^{2+} release but decreased mitochondrial O_2 consumption and mtDNA depletion in β*Mfn1/2*-KO islets. Agonism at the Gq-coupled metabotropic acetylcholine (Ach) receptor in β-cells results in the production of inositol (1,4,5)trisphosphate (IP_3) which, in turn, triggers rapid release of Ca^{2+} from the ER (Gilon, Chae et al. 2014). Since MFN2 is implicated in the control of ER-mitochondria interactions (Filadi, Greotti et al. 2017) cytosolic Ca^{2+} dynamics were again recorded in whole islets using Cal-520. These experiments did not reveal any differences in apparent ER Ca^{2+} release between groups following Ach treatment (Fig.**4A-B**), arguing against a substantial impact on ER-mitochondria contacts.

Given the marked alterations in mitochondrial morphology, cristae structure and glucose-induced changes in ATP/ADP ratio in KO cells described above, we decided to pursue further assessments of mitochondrial function using orthogonal approaches. Measurements of O_2 consumption revealed that both basal and glucose-stimulated mitochondrial respiratory capacities were significantly impaired in β*Mfn1/2*-KO islets, as reflected by the calculated AUC values ($p < 0.05$;Fig.**4C-D**). Consistent with these reduced rates of respiration, KO islets also displayed a ~75% reduction in mtDNA (Fig.**4E**).

β*Mfn1/2*-KO mice display impaired GSIS *in vitro* and insulin vesicle exocytosis which can be rescued by incretins. We next explored the consequences of *Mfn1/2* deletion for glucose-stimulated insulin secretion (GSIS), as well as secretion stimulated by other agents, by comparing islets isolated from WT and β*Mfn1/2*-KO mice. With respect to WT controls, KO islets exhibited a sharp blunting in the secretory response to high glucose, as well as to depolarisation with KCl. In each case, a near-complete elimination of insulin secretion in response to stimulation was observed ($p<0.05$;$p<0.01$;Fig.**4F**). However, ncubation of islets with incretins (GLP-1 or GIP), or the GLP1R agonist exendin-4, at 10 mmol/L glucose led to a significant potentiation in GSIS in both groups (WT: 3G vs ex-4; $p<0.05$ and KO: 3G vs ex-4; $p<0.0001$, or 3G vs GLP-1; $p<0.001$, or 3G vs GIP; $p<0.001$). Strikingly, these results revealed the rescue of robust insulin secretion by incretins in β*Mfn1/2*-KO islets.

Finally, total internal reflection fluorescence (TIRF) was adopted to image insulin granule trafficking and exocytosis in dissociated β-cells. By over-expressing the secretory vesicle marker neuropeptide Y-Venus (NPY-Venus), the number of insulin

granules was quantified by confocal microscopy and revealed a significantly higher number of vesicles in close proximity with the plasma membrane in KO cells after treatment with 20 mmol/L KCl ($p<0.05$; Suppl.Fig.**4A-B).** However, when we then used a cell surface-targeted zinc indicator to monitor induced exocytotic release (ZIMIR) in response to depolarisation as a surrogate for insulin secretion, weaker increases were observed in KO mouse β-cells. These findings indicate impaired exocytosis at the plasma membrane of an otherwise normal or increased pool of docked granules (Suppl.Fig.**4C-E**).

***Mitofusin* deletion leads to increased β-cell death and reduced β-cell mass.** Immunohistochemical analysis of pancreata from mice sacrificed at 14 weeks showed that removal of *Mfn1* and *Mfn2* caused a significant (~33%) loss of pancreatic beta (insulin-positive) cells in the KO vs the WT group ($p<0.05$; Fig.**5A-B**). Alpha (glucagon-positive) cell surface was not affected by the loss of the mitofusin genes (Fig.**5C**). However, *Mfn1* and *Mfn2* loss was associated with a ~53% reduction in β-cell-alpha cell ratio ($p<0.05$; Fig.**5D**). In line with these findings, the number of TUNEL-positive β-cells were markedly increased in β-cells from β*Mfn1/2*-KO vs WT animals ($p<0.05$; Fig.**5E-F**), suggesting that programmed cell death contributes to the observed decrease in β-cell mass.

Gene dysregulation in β*Mfn1/2*-KO islets. We next explored whether the defects in β-cell secretory function could potentially be due to impaired expression of “signature” genes, known to be vital for β-cell differentiation and function, or to increased expression of β-cell “disallowed” genes (Pullen, Huising et al. 2017). Measurements of these, alongside genes involved in mitophagy and ER stress, in WT and KO islets

indicated that β-cell function was affected at the transcriptional level in β*Mfn1/2*-KO mice (Fig.**6**). Whilst *Ins2*, *Ucn3* and *Glut2* (*Slc2a2*) were significantly downregulated, *Trpm5* was upregulated, in KO islets. No changes in alpha or β-cell disallowed genes were detected. In contrast, genes involved in mitochondrial function such as *Smdt1* and *Vdac3* were upregulated in β*Mfn1/2*-KO islets, consistent with compromised mitochondrial Ca^{2+} uptake, and ATP release, respectively, in KO β-cells. Lastly, genes involved in ER stress and mito/autophagy were also affected by inactivation of *Mfn1* and *Mfn2* with *Chop (Ddit3)* and *p62* being upregulated and *Lc3* and *Cathepsin L* downregulated in KO islets.

Altered plasma metabolomic and lipidomic profiles in β*Mfn1/2*-KO mice. We applied an -omics approach to study metabolite and lipid changes in peripheral plasma samples from WT and KO mice (Suppl.Fig.**5**). Of 29 metabolites, the levels of five metabolic species (shown in red) were significantly altered in β*Mfn1/2*-KO compared to WT animals ($p<0.05$;$p<0.01$;Suppl.Fig.**5A**). More precisely, bile acids such as glycocholic acid (GCA), taurocholic acid (TCA) and taurodeoxycholic/taurochenodeoxycholic acid (TDCA/TCDCA) involved in the emulsification of fats were found upregulated in KO mice. Leucine (Leu) and isoleucine (Ile) were also upregulated in KO mice. In this lipidomics analysis, 298 lipid species from 17 different classes were studied. When comparing KO to WT samples, the majority of lipid classes displayed a remarkably homogeneous downward trend of the individual lipid species they comprised (Suppl.Fig.**5B**). Most prominently, plasma concentrations of lipids within the Cer, PC, PC(P-)/PC(O-), PE (O-), PI, SM and LPC classes were significantly less abundant in KO than WT mice ($p<0.05$;$p<0.01$; Suppl.Fig.**5B**).

Glucose-induced cytosolic Ca^{2+} and $\Delta\psi_m$ changes are impaired in β*Mfn1/2*-KO β-cells *in vivo.* To further explore the extent to which defective mitochondrial membrane polarisation and Ca^{2+} dynamics observed in isolated islets were likely to underlie the defects in insulin secretion *in vivo*, two-photon imaging was used to allow visualisation of the intact pancreas, exposed through an abdominal incision, in anaesthetised mice (Reissaus, Piñeros et al. 2019). Animals previously infected with an adenovirus expressing the Ca^{2+} probe GCaMP6s, and co-stained with tetramethyl rhodamine methyl ester (TMRM) immediately prior to data capture, were imaged for 18-30 min. during which cytosolic Ca^{2+} oscillations and mitochondrial membrane potential were recorded post i.p. injection of glucose in WT (Fig.**7A**; Suppl.Fig.**6A**) and KO (Fig.**7B**; Suppl.Fig.**6B**) mice. Under these conditions, glucose concentrations in WT mice were 17.1±2.5 mmol/L and 32.1±3.9 mmol/L in KO animals after glucose injection. Analysis was performed on the most responsive β-cells where oscillations could be detected in both groups and revealed cytosolic Ca^{2+} oscillations (upward traces) and synchronous mitochondrial membrane depolarisation (downward traces; TMRM positive organelles) in response to elevated glucose in WT β-cells. On the other hand, cytosolic Ca^{2+} oscillations and TMRM fluctuations were largely abolished in β*Mfn1/2*-KO islets in response to glucose (Fig.**7B**;Suppl.Fig.**6B**). Measurement of the AUC of fold change traces above baseline depicted significantly impaired GCaMP6s spike signals in response to glucose (Fig.**7C**;$p<0.001$ and $p<0.05$; Suppl.Fig.**6C**) and a tendency towards less TMRM (Fig.**7D**) uptake in β*Mfn1/2*-KO islets.

Changes in *Mfn1* and *Mfn2* expression in mouse strains maintained on regular chow or high fat high sugar (HFHS) diet. To determine whether the expression of

Mfn1 or *Mfn2* might be affected under conditions of hyperglycaemia mimicking T2D in man, we interrogated data from a previous report (Cruciani-Guglielmacci, Bellini et al. 2017) in which RNA sequencing was performed on islets from six mouse strains (C57Bl/6J, DBA/2J, BALB/cJ, A/J, AKR/J, 129S2/SvPas). Animals were maintained on regular chow or a high fat/high sugar diet (Suppl.Fig.**7A-B**). BALB/cJ mice showed "antiparallel" changes in *Mfn1* and *Mfn2* expression in response to maintenance on HFHS diet for 10 days, and similar changes were obtained in DBA/2J mice at 30 and 90 days (Suppl.Fig.**7A-B**).

Discussion

Mitochondrial dynamics contribute to the maintenance of a metabolically-efficient mitochondrial population, with an impaired balance between fusion and fission impacting mitochondrial morphology and functionality. To date, dynamic and bioenergetic mitochondrial defects have been explored in conditional KO mouse models where different organs such as the liver, skeletal muscle, adipocyte, heart, nervous system, placenta and optic nerve were examined (Eisner, Picard et al. 2018).

A number of studies have demonstrated that mitochondrial dysfunction contributes to the deterioration of β-cell function and the development of T2D (Maechler and Wollheim 2001, Anello, Lupi et al. 2005, Lowell and Shulman 2005, Dlaskova, Spacek et al. 2010, Haythorne, Rohm et al. 2019). Deletion of *Drp1* from primary mouse β-cells resulted in glucose intolerance, with impaired GSIS and abnormal mitochondrial morphology associated with lower expression of MFN1, MFN2 and OPA1 (Reinhardt, Schultz et al. 2016, Hennings, Chopra et al. 2018). Similarly, over-expression of DRP1 in clonal INS1 cells decreased GSIS and increased the levels of apoptosis (Stiles and Shirihai 2012), suggesting that a balance between fission and fusion is critical to avoid pathological changes. In line with these data, mice deficient for *Opa1* in the β-cell develop hyperglycaemia, and show defects in the electron transport chain complex IV which lead to compromised glucose-stimulated ATP production, O_2 consumption, Ca^{2+} dynamics, and insulin secretion (Zhang, Wakabayashi et al. 2011).

The chief aim of this study was to determine the impact of compete ablation of MFN activity from the β-cell. We report that deletion of both mitofusin isoforms, *Mfn1* and *Mfn2*, leads to a profound disruption of β-cell function and identity. This strategy was chosen over the deletion of either gene alone given the similar levels of expression of

these genes in the β-cell (Kone, Pullen et al. 2014) and the likelihood of at least partial functional redundancy (Filadi, Pendin et al. 2018). Through the highly efficient and selective ablation of *Mfn1* and *Mfn2* in adult pancreatic β-cells, we reveal that an intact mitochondrial network is essential to maintain normal insulin secretion and circulating glucose levels.

Deletion of *Mfn1/2* ensured near-complete elimination of the mRNA encoding *Mfn1* and *Mfn2* throughout the β-cell population while MFN1 and MFN2 protein expression was completely abolished. As a consequence, β*Mfn1/2*-KO mice lost significant body weight 14 weeks post tamoxifen injection, consistent with the onset of hyperglycaemia and diabetes. In agreement with earlier studies (Maechler and Wollheim 2001, Anello, Lupi et al. 2005, Lowell and Shulman 2005, Dlaskova, Spacek et al. 2010), where altered mitochondrial dynamics were shown to affect β-cell function, GSIS post i.p. injection *in vivo,* or in isolated islets *in vitro,* was severely compromised in the present model. Reduced insulin exocytotic activity measured by TIRF indicated that KO β-cells fail to respond to glucose or depolarising factors, leading to impaired glucose clearance and hyperglycaemia during IPGTTs. Insulin secretion was nevertheless potentiated following exposure to incretin hormones or GLP1R agonists suggesting that signalling by the latter receptors may restore β-cell responsiveness to glucose in diabetic mice (Nauck and Meier 2018). Future investigations will be needed to better understand the underlying mechanisms. However, since cAMP levels are required for efficient insulin secretion (Pipeleers, in't Veld et al. 1982) and may be lowered in KO islets as a result of ATP depletion, a likely possibility is that incretin stimulation is required to raise intracellular cAMP levels to the threshold levels needed for secretion (Khan, Tomas et al. 2020).

We assessed how mitochondrial morphology was affected in β*Mfn1/2*-KO β-cells using complementary strategies. Firstly, quantitative analysis of deconvolved confocal images revealed distinct and more rounded organelles in the KO group compared to WT littermates where web-like mitochondrial networks were often apparent. Secondly, TEM confirmed mitochondrial fragmentation in isolated islets and, interestingly, revealed a marked alteration in cristae shape and structure in KO mice. Mitochondrial adaptation to altered physiological conditions relies on the regulation of mitochondrial morphology, especially at the level of cristae compartment (Quintana-Cabrera, Mehrotra et al. 2018). Since cristae shape determines the assembly and stability of the respiratory chain complexes (Cogliati, Frezza et al. 2013), loss of the latter is associated with lowered respiratory chain efficiency, as observed directly in respirometry measurements. These findings are also in line with our observation of lowered mtDNA copy number in KO islets (Silva, Köhler et al. 2000).

Under normal conditions, glucose-induced increases in cytosolic Ca^{2+} in β-cells stimulate insulin exocytosis by inducing closure of K_{ATP}-channels, plasma membrane depolarisation and Ca^{2+} influx (Ashcroft and Rorsman 2013, Rutter, Pullen et al. 2015). This pathway appears to be inhibited in KO islets both *in vivo* and *in vitro*. We also demonstrate here that mitochondrial ultra-structure is important for normal β-β-cell connections which are, in turn, essential for coordinated Ca^{2+} influx into β-cells and ultimately, efficient and oscillatory insulin secretion (Salem, Silva et al. 2019). Thus, the strength of coordinated β-cell responses at 17 mmol/L glucose, assessed using Pearson *r* analysis, was lowered in β*Mfn1/2*-KO mice. The mechanisms underlying these changes are, however, unclear and were not associated with any changes in

Cx36/Gjd2 gene expression required to form gap junctions between β-cells (Rutter, Georgiadou et al. 2020). Furthermore, these changes were not associated with any loss of hierarchical behaviour or the loss of a more highly connected "hub" cell population.

Immunofluorescence analysis showed reduced β-cell volume (the ratio of β-cell over total pancreas area) in KO islets describing the occurrence of β-cell loss and dysfunction in T2D (Butler, Janson et al. 2003). The underlying mechanisms remain to be fully elucidated but appear to involve a dramatic increase in β-cell apoptosis (Marchetti, Del Guerra et al. 2004) though we do not exclude altered β-cell replication or neogenesis (Butler, Janson et al. 2003) as contributors. Previous studies have raised a number of potential mechanisms by which mitochondrial fragmentation can affect apoptosis (Frank, Gaume et al. 2001, Olichon, Baricault et al. 2003). Fragmentation occurs early in the cell death pathway (Heath-Engel and Shore 2006) and is thought to contribute to cytochrome *c* production and release into the cytosol, decrease in O_2 consumption and thereby, enhancing oxidative stress (Molina, Wikstrom et al. 2009).

Loss of β-cell identity is now thought to be a key element driving impaired β-cell function in T2D (Talchai, Xuan et al. 2012, Rutter, Pullen et al. 2015) and may underlie impaired insulin secretion from remaining β-cells in type 1 diabetes (Rui, Deng et al. 2017). As GSIS was almost completely eliminated *in vivo* and *in vitro* after *Mfn1/2* deletion in the β-cell, despite only partial loss of β-cells, our data support the view that a similar change may contribute to functional alterations in the current model. Whilst we observed decreases in *Ins2*, *Ucn3* and *Glut2/Slc2a2* expression, *Trpm5* was

upregulated in KO islets. This denotes that β-cell maturation (UCN3) as well as function (glucose uptake through GLUT2/SLC2A2), insulin production (*Ins2*) and β-cell plasma membrane excitability (TRPM5) were all affected when mitochondrial fusion was repressed. Thus, the mitochondrial abnormalities in *Mfn1/2*-deficient β-cells appear to affect β-cell identity, leading to metabolic derangement and defective secretion. We note that the progressive hyperglycaemia that ensues may further aggravate dedifferentiation (Brereton, Iberl et al. 2014) and lead to changes in β-cell transcription factor expression (Yin, Ni et al. 2020). No changes in inactivated ("disallowed") β-cell gene levels were detected in *Mfn*1/2-deficient mice, suggesting that mitochondrial structure alterations do not affect disallowed gene expression, at least in young mice.

Moreover, genes encoding mitochondrial channel subunits such as *Smdt1* and *Vdac3* were upregulated in β*Mfn1/2*-KO mice suggesting that mitochondrial Ca^{2+} uptake via the mitochondrial Ca^{2+} uniporter (MCU) subunit EMRE (Georgiadou, Haythorne et al. 2020), encoded by *Smdt1*, and extrusion of ATP through VDAC3 (Maldonado, Sheldon et al. 2013) are impacted when mitochondria are highly fragmented. Lower *Vdac3* expression is also linked to mitochondrial permeability transition pore (mPTP) opening (Reina, Guarino et al. 2016) and hence could be a driver of increased apoptosis. Lastly, genes involved in ER stress and mito/autophagy were also altered in β*Mfn1/2*-KO mice, with *Chop/Ddit3* and *p62* being upregulated and, *Lc3* and *Cathepsin L* downregulated. These results demonstrate that highly fragmented mitochondria undergo ER stress but are unable to enter the autophagosome-lysosome pathway in order to eliminate dysfunctional mitochondria and avoid β-cell apoptosis (Sidarala, Pearson et al. 2020).

It has previously been reported that ER overload triggers ER stress through *Chop* overexpression and can lead to increased β-cell apoptosis and the onset of diabetes in mice (Araki, Oyadomari et al. 2003, Song, Scheuner et al. 2008). Additionally, and although we did not observe any changes in the expression of the mitophagy inducers *Pink1*/*Parkin* (Gegg, Cooper et al. 2010), the autophagy adaptor gene *p62,* which mediates the clearance of dysfunctional mitochondria via macroautophagy (Tanida and Waguri 2010), was upregulated at the mRNA level. These elevated levels of ubiquitin and p62 may conceivably lead to the formation of proteinaceous aggregates and ultimately cell death (Komatsu, Waguri et al. 2007). Finally, reduction in *Lc3* gene expression known to contribute to the autophagosome body formation (Tanida and Waguri 2010) and in lysosomal proteases (*Cathepsin L*), known to degrade macromolecules contained in autophagolysosomes (Tanida and Waguri 2010) further confirm our speculations that dysfunctional regulation of autophagic processes can lead to increased β-cell death, as demonstrated in β*Mfn1/2*-KO pancreatic sections.

Since quantitative determination of plasma metabolites may be informative about pathogenic conditions, we searched for metabolite species related to diabetes, complications and metabolic dysfunction while the lipid platform detected lipids to a fullest extent. Metabolomic analysis of the plasma of WT and KO mice identified a higher synthesis rate of certain bile acids in β*Mfn1/2*-KO animals which correlated with published work stating that bile acid pool size and composition can be altered in T2D animal models or human patients (Hassan, Subbiah et al. 1980, Andersén, Karlaganis et al. 1988, Staels and Fonseca 2009). More precisely, in obese and insulin resistant Zucker diabetic fatty (ZDF) rats, hepatic farnesoid X receptor (FXR) expression decreased in parallel with diabetes progression while a progressive increase of liver

cholesterol-7α-hydroxylase (*Cyp7a1*) expression, involved in bile acid synthesis, was observed (Duran-Sandoval, Mautino et al. 2004). This study suggested that the increased bile acid synthesis observed in ZDF rats was a consequence of a lack of negative insulin-mediated regulation of genes encoding bile acid synthesis enzymes and could hence, also be the case in our mouse model. Additionally, leucine and isoleucine known to acutely stimulate insulin secretion and improve glycaemia when administrated to humans or rodents (Yang, Chi et al. 2010) were found to be higher in β*Mfn1/2*-KO animals. This may imply that potentiation of the iso/leucine mediated signalling pathway is required to acutely induce insulin secretion stimulation and serve as a rescue mechanism in β*Mfn1/2*-KO mice. It may also influence the mechanistic target of rapamycin (mTOR) complex 1 (mTORC1) activity and indicate changes in mitochondrial fuel preference/utilization (McDaniel, Marshall et al. 2002, Kwon, Marshall et al. 2004).

Similar to findings in other population-based studies on T1 and T2D patients, our mouse lipid profile supports a liver fatty acid synthesis perturbation and could be a factor associated with impaired glucose tolerance and altered insulin secretion (Sorensen, Ding et al. 2010, Lamichhane, Ahonen et al. 2018). In particular, we found that the Cer, PC, PC(P-)/PC(O-), PE (O-), PI, SM and LPC class lipids were lower in β*Mfn1/2*-KO mice compared to WT. Finally, the reduction of certain lipids could indicate an increase in fatty acid β-oxidation in order to produce sufficient energy to sustain the energy demand of peripheral tissues and, hence, explain why an increase in circulating ketone bodies is observed in KO mice.

In conclusion, we provide evidence here that an altered balance of mitochondrial fusion and fission has a drastic impact on β-cell function. Our findings establish an

important role for β-cell *Mfn1* and *Mfn2* in regulating plasma glucose levels, GSIS, islet Ca^{2+} oscillations and β-cell death. Importantly, changes in the expression of both genes were observed in two mouse models of diabetes, suggesting that similar changes might be involved in human diabetes. Although we are not aware of reports of changes in the expression of either gene in this setting, we note that measurements at the protein level may be important given the possibility that post-translational changes may contribute. Importantly we show that treatment with incretins, commonly used as treatments for T2D and obesity (Nauck and Meier 2018), is able largely to reverse the deficiencies in insulin secretion, suggesting that this may be an important mechanisms of action of this drug class.

Acknowledgements

We thank Stephen M. Rothery from the Facility for Imaging by Light Microscopy (FILM) at Imperial College London for support with confocal and widefield microscopy image recording and analysis. We also thank Aida Di Gregorio from the National Heart and Lung Institute (Imperial College) for genotyping the mice.

Funding

GAR was supported by a Wellcome Trust Senior Investigator Award (WT098424AIA) and Investigator Award (212625/Z/18/Z), MRC Programme grants (MR/R022259/1, MR/J0003042/1, MR/L020149/1), an Experimental Challenge Grant (DIVA, MR/L02036X/1), an MRC grant (MR/N00275X/1), and a Diabetes UK grant (BDA/11/0004210, BDA/15/0005275, BDA16/0005485). IL was supported by a Diabetes UK project grant (16/0005485). This project has received funding from the Innovative Medicines Initiative 2 Joint Undertaking, under grant agreement no. 115881 (RHAPSODY). This Joint Undertaking receives support from the European Union's Horizon 2020 research and innovation programme and EFPIA. This work is supported by the Swiss State Secretariat for Education, Research and Innovation (SERI), under contract no. 16.0097. AT was supported by MRC project grant MR/R010676/1. Intravital imaging was performed using resources and/or funding provided by National Institutes of Health grants R03 DK115990 (to AKL), Human Islet Research Network UC4 DK104162 (to AKL; RRID:SCR_014393).

Author contributions

EG performed experiments and analysed data. EG supported the completion of confocal and widefield microscopy and analysis. ATC performed the EM sample

processing and data analysis. CM, MM and AKL were responsible for the *in vivo* intravital Ca^{2+} imaging in mice. PC contributed to the analysis and manipulation of the *in vivo* intravital Ca^{2+} measurements as well as the preparation and imaging of TIRF samples. TS contributed to the generation of the MATLAB script used for connectivity analysis. FYSW and YA generated and performed Monte Carlo-based signal binarisation. NA assisted with Seahorse experiment protocols. CLQ and AW contributed to the metabolomics analysis. CCG, CM and MI were responsible for the RNAseq data analysis. TAR was involved in the design of the floxed *Mfn* alleles. TAR and IL were responsible for the maintenance of mouse colonies and final approval of the version to be published. GAR designed the study and wrote the manuscript with EG with input and final approval of the version to be published from all authors. GAR is the guarantor of this work and, as such, had full access to all the data in the study and takes responsibility for the integrity of the data and the accuracy of the data analysis.

Declaration of interests

Authors' relationships and activities GAR has received grant funding and consultancy fees from Les Laboratoires Servier and Sun Pharmaceuticals. The remaining authors declare that there are no relationships or activities that might bias, or be perceived to bias, their work.

Figure legends

Fig.1 Generation of a conditional βMfn1/2-KO mouse line which displays a highly impaired glucose tolerance *in vivo*.(A) qRT-PCR quantification of *Mfn1, Mfn2, Drp1, Opa1* and *Fis1* expression in WT (*Mfn1/2* $^{+/+}$) and β*Mfn1/2*-KO (*Mfn1/2* $^{-/-}$) islets relative to *β-actin* (*n*=3-5 mice per genotype in two independent experiments).(B) Western blot analysis demonstrating efficient MFN1 (84 kDa) and MFN2 (86 kDa) deletion relative to GAPDH (36 kDa) in isolated islets (*n*=3-4 mice per genotype in three independent experiments).(C) Glucose tolerance was measured in *Mfn1/2* $^{-/-}$ mice and littermate controls (*Mfn1/2* $^{+/+}$) by IPGTT (1 g/kg body weight).(D) The corresponding AUC is shown for *n*=3-6 mice per genotype.(E) Glucose tolerance measured by IPGTT (using 3 g/kg body weight) and (F) the corresponding AUC were assessed in β*Mfn1/2*-KO and WT mice (*n*=3-6 mice per genotype).(G) Plasma insulin levels during IPGTT in KO and WT mice (*n*=3-6 mice per genotype) and (H) the corresponding AUC.(I) Challenging β*Mfn1/2*-KO mice with a 0.75 U/kg body weight insulin injection as compared with WT mice.(J) Corresponding AUC for (I) is also shown (*n*=6 mice per genotype).(Blue, *Mfn1/2* $^{+/+}$ mice; red, *Mfn1/2* $^{-/-}$ mice. Data are presented as mean±SEM. *p<0.05; **p<0.01; ***p<0.001; ****p<0.0001 as indicated or *Mfn1/2* $^{+/+}$ vs *Mfn1/2* $^{-/-}$ mice at the time points indicated, analysed by unpaired two-tailed Student's t-test and Mann–Whitney correction or two-way ANOVA test and Sidak's multiple comparisons test.

Fig.2 Mitochondrial ultrastructure is altered following *Mfn1/2* deletion.(A) Confocal images of the mitochondrial network of dissociated β-cells stained with Mitotracker green; scale bar: 5 μm. Lower right panels: magnification of selected areas.(B) Mitochondrial morphology analysis on deconvolved confocal images of dissociated β-cells. A macro was developed to quantify the number of mitochondria per cell and measure the elongation, perimeter and circularity (0: elongated; 1: circular mitochondria) of the organelles in WT and KO animals (*n*=40-54 cells; *n*=3 mice per genotype).(C) Electron micrographs of mitochondria indicated with black arrows in islets isolated from *Mfn1/2* $^{+/+}$ and *Mfn1/2* $^{-/-}$ mice; scale bars: 1μm. Right panel: magnification of selected areas showing the cristae structure (black arrow heads); scale bar: 0.5 μm. Schematic representation of enlarged mitochondria. Data are

presented as mean±SEM. ****p<0.0001 as indicated, analysed by unpaired two-tailed Student's t-test and Mann–Whitney correction.

Fig.3 *Mfn1/2* deletion from pancreatic β-cells impairs cytosolic and mitochondrial Ca^{2+} uptake and changes mitochondrial potential and ATP synthesis *in vitro*.(A) $[Ca^{2+}]_{cyt}$ changes in response to 3G, 3 mmol/L glucose, 17 mmol/L glucose (17G; with or without diazoxide [diaz]) or 20 mmol/L KCl with diaz were assessed following Cal-520 uptake in whole islets. Traces represent mean normalised fluorescence intensity over time (F/F_{min}).(B) The corresponding AUC is also presented (*n*=4 mice per genotype; 17G AUC measured between 245 s and 1045 s, 17G+diaz AUC measured between 1200 s and 1320 s), and KCl+diaz AUC measured between 1424 s and 1500 s).(C) $[Ca^{2+}]_{mito}$ changes in response to 17G (with or without diazoxide [diaz]) and 20 mmol/L KCl were assessed in islets following R-GECO infection. Traces represent mean normalised fluorescence intensity over time (F/F_{min}).(D) The corresponding AUC is also shown (*n*=3 mice *per* genotype; 17G AUC measured between 270 s and 1100 s, 17G+diaz AUC measured between 1101 s and 1365 s and KCl AUC measured between 1366 s and1500 s).(E) Dissociated β-cells were loaded with TMRE to measure changes in $\Delta\psi_m$, and perifused with 3 mmol/L glucose (3G), 17G or FCCP as indicated. Traces represent normalised fluorescence intensity over time (F/Fmin).(F) AUC was measured between 700–730 s (under 17G exposure) from the data shown in (E).(G) Changes in the cytoplasmic ATP:ADP ratio ([ATP:ADP]) in response to 17 mmol/L glucose (17G) was examined in whole islets using the ATP sensor Perceval.(H) AUC values corresponding to (G) were measured between 418–1400 s (under 17G exposure) (data points from *n*=3-6 mice per genotype). Data are presented as mean±SEM. *p<0.05, **p<0.01, assessed by unpaired two-tailed Student's t-test and Mann–Whitney correction or two-way ANOVA test and Sidak's multiple comparisons test.

Fig.4 O_2 consumption and mtDNA are deleteriously affected when *Mfn1/2* are abolished in β-cells, while $[Ca^{2+}]_{ER}$ storage remains unchanged. Impaired insulin secretion can be rescued by GLP-1R agonists *in vitro*.(A) Changes in $[Ca^{2+}]_{ER}$ were measured in whole islets incubated with Cal-520 and perifused with 17 mmol/L glucose (17G; with or without diazoxide [diaz]), 17G with 0.1mmol/L acetylcholine (Ach) and diaz, or 20 mmol/L KCl with diaz (B) AUC values corresponding to (A) were

measured (17G AUC measured between 260 s and 740 s, 17G+diaz AUC measured between 846 s and 1020 s, 17G+diaz+Ach AUC measured between 1021 s and 1300 s and KCl AUC measured between 1301 s and 1500 s). (C) Representative oxygen consumption rate (OCR) traces of islets (~10 per well) were acutely exposed to 20 mM glucose (final concentration), Oligomycin A (Oligo), FCCP, and Rotenone with Antimycin A (AA) (performed in triplicate, in two independent experiments).(D) AUC values corresponding to (C).(E) The relative mitochondrial DNA copy number was measured by determining the ratio of the mtDNA-encoded gene *mt-Nd1* to the nuclear gene *Ndufv1* (*n*=3 mice per genotype).(F) Insulin secretion measured during serial incubations in batches in 3 mmol/L glucose (3G), 10 mmol/L glucose (10G), or 100 nmol/L exendin-4 (ex-4), GLP-1 or GIP in presence of 10G, 17 mmol/L glucose (17G) or 20mmol/L KCl (*n*=4-7 mice per genotype in two independent experiments).Data are presented as mean±SEM. *p<0.05, assessed by unpaired two-tailed Student's t-test and Mann–Whitney correction or two-way ANOVA test and Sidak's multiple comparisons test.

Fig.5 Absence of *Mfn1/2* in β-cells leads to decreased β-cell mass and increased β-cell apoptosis.(A) Representative pancreatic sections immunostained with glucagon (red) and insulin (green); scale bars: 30-50μm.(B) The β-cell and alpha cell surface (C) measured within the whole pancreatic area in WT and KO mice were determined, as well as the beta/alpha cell ratio in (D), (*n*=4 mice per genotype; experiment performed in triplicate).(E) Representative confocal images of islets with TUNEL positive (green) apoptotic β-cells (white arrows) and insulin (red). DNase I treated sections were used as a positive control in the TUNEL assay. Scale bars: 20μm.(F) Quantification of the percentage of islets containing TUNEL positive cells (*n*=4 mice per genotype; experiment performed in triplicate). Data are presented as mean±SEM. *p<0.05, assessed by unpaired two-tailed Student's t-test and Mann–Whitney correction.

Fig.6 Heatmap of differential gene expression between β*Mfn1/2*-KO and WT islet mRNA. Changes in key beta or alpha cell genes, disallowed genes, mitochondrial, ER stress or mito/autophagy genes were assessed by qRT-PCR in WT and KO islets according to the colour coded median values from 0 to 1, white to dark blue

respectively (*n*=3-4 mice per genotype; experiment performed in duplicate). Expression values for each gene were normalised to *β-actin*. *p<0.05; **p<0.01, assessed by two-way ANOVA test and Sidak's multiple comparisons test.

Fig 7. Deletion of Mfn1/2 impairs β-cell function *in vivo*. Representative *in vivo* images of GCaMP6s labelled islets and TMRM stained mitochondria surrounded by their vasculature in WT and β*Mfn1/2*-KO mice.(A) Representative traces depicting fluorescence intensity of cytosolic Ca^{2+} (GCaMP6s) and mitochondrial TMRM signals in WT and (B) KO animals; scale bar: 45 μm; (*n*=2 animals per genotype).(C) AUC of fold change measurements above baseline for each GCaMP6s and (D) TMRM traces measured (*n*=4-15 total responding cells). Green, GCaMP6s; red, TMRM signals. Islets were imaged in 20 week-old mice. Data are presented as mean±SEM. ***p<0.001, assessed by unpaired two-tailed Student's t-test and Mann–Whitney correction.

STAR Methods

Study approval C57BL/6J mice were housed in individually ventilated cages in a pathogen-free facility at 22ºC with a 10-14 h light-dark cycle and were fed *ad libitum* with a standard mouse chow diet (Research Diets). All *in vivo* procedures were approved by the UK Home Office, according to the Animals (Scientific Procedures) Act 1986 with local ethical committee approval under personal project license (PPL) number PA03F7F07 to I.L.

Generation of β-cell-selective *Mfn1/Mfn2* knockout (β*Mfn1/2*-KO) mice

C57BL/6J male mice bearing *Mfn1* ($Mfn1^{tm2Dcc}$; JAX stock #026401) and *Mfn2* (B6.129(Cg)-$Mfn2^{tm3Dcc}$/J; JAX stock #026525) alleles (Chen, McCaffery et al. 2007) with *lox*P sites flanking exons 4 and 6 were purchased from the Jackson laboratory and crossed to C57BL/6J transgenic animals carrying an inducible *Cre* recombinase under *Pdx1* promoter control (Pdx1-Cre^{ERT2}) (Gu, Dubauskaite et al. 2002). Mice bearing floxed *Mfn* alleles but lacking *Cre* recombinase were used as WT littermate controls. Mice were genotyped following protocols described by the Jackson laboratory for each of these strains. (See Electronic Supplemental Material (ESM) Table 1 for genotyping primer details). Recombination was achieved by daily tamoxifen (20mg/ml [diluted in corn oil; Sigma]) i.p. injections for five days at 7-8 weeks of age. Body weight was monitored every week, for 14 weeks, in *ad libitum* fed mice. Unless otherwise stated, all experiments were performed on 14-weeks aged male mice.

mRNA extraction and quantitative reverse transcription PCR For measurements of mRNA levels, pancreatic islets from WT and β*Mfn1/2*-KO mice were isolated by

collagenase digestion (Ravier and Rutter 2010). Total RNA from islets (50-100) was extracted using Trizol according to the manufacturer's instructions. RNA (100-200ng) was then reverse transcribed using the High-Capacity cDNA reverse transcription kit (Life Technologies) including random primers. Gene expression was determined by quantitative reverse transcription PCR (qRT-PCR) using a SYBR Green PCR master mix (Life Technologies) and normalised to *β-actin* (Georgiadou, Haythorne et al. 2020) (see ESM Table 2 for primer details).

Tissue DNA extraction and measurement of mitochondrial DNA (mtDNA) copy number Total islet DNA was isolated using Puregene Cell and Tissue Kit (Qiagen) and was amplified (100ng) using NADH dehydrogenase I primers (Kolesar, Wang et al. 2013), also known as complex I (*mt9/mt11)* for mtDNA and *Ndufv1* for nuclear DNA by real-time PCR using the Power SYBR Green RT-PCR kit (Applied Biosystems). The mtDNA copy number was calculated using *Ndufv1* amplification as a reference for nuclear DNA content.

SDS-PAGE and western blotting After isolation, ~100 islets were collected and lysed in ice-cold buffer (150 mmol/L NaCl, 10 mmol/L Tris HCl pH 7.2, 0.1% SDS, 1% sodium deoxycholate, 5 mmol/L EDTA, 1% Triton X-100) containing protease inhibitor cocktail (Roche) and phosphatase inhibitors (Sigma-Aldrich). 20 µg of total proteins were loaded, according to bicinchoninic acid (BCA) assay (Thermo Fisher) quantification. Lysates were denatured and resolved by 12% SDS-PAGE,and transferred to poly-vinylidene fluoride (PVDF) membranes (GE Healthcare) before immunoblotting. Blots were blocked 1 h at room temperature (RT) with 5% non-fat dry milk (Sigma-Aldrich) in TBS-tween (10 mmol/L Tris, 150 mmol/L NaCl, 0.1% Tween

20) solution and incubated at 4 °C with the primary antibody. Secondary antibodies were incubated 2 h at RT. Antibodies used in Western (immuno-) blot analysis were the following: mouse anti-MFN1 (Abcam, ab126575, RRID:AB_11141234, 1:500), mouse anti-MFN2 (Abcam, ab56889, RRID:AB_2142629, 1:500), goat anti-rabbit GAPDH (Cell signalling, #2118s, RRID:AB_561053; 1:10 000), goat anti-mouse HRP (Abcam, ab205719, RRID:AB_2755049, 1:5 000).

Intraperitoneal (i.p.) glucose or insulin tolerance test and measurement of insulin secretion or ketone levels *in vivo* For glucose tolerance tests (IPGTT), WT and β*Mfn1/2*-KO mice were fasted overnight followed by i.p. injection of glucose (20% w/v, 1g/kg body weight). Insulin tolerance was assessed 4 hours post-fasting and injection of insulin (0.75U/kg; Eli Lilly) i.p. (IPITT). Glucose was measured in tail vein blood at time points as indicated using an ACCU-CHECK Aviva glucometer (Roche). For *in vivo* insulin secretion measurements, fasted mice (overnight) were administered glucose (20% w/v, 3g/kg body weight) i.p., and plasma insulin was measured using an ultra-sensitive mouse insulin enzyme-linked immunosorbent assay (ELISA) kit (CrystalChem). β-ketones were measured in tail vein blood from fed or fasted (16h) mice using an Area 2K device (GlucoMen).

***In vitro* insulin secretion** Islets were isolated from mice and incubated for 1 h in Krebs-Ringer bicarbonate buffer (140 mmol/L NaCl, 3.6 mmol/L KCl, 0.5 mmol/L NaH_2PO_4, 2 mmol/L $NaHCO_3$ [saturated with CO_2], 1.5 mmol/L $CaCl_2$, 0.5 mmol/L $MgSO_4$, 10 mmol/L HEPES; pH 7.4) containing 3 mmol/L glucose. Subsequently, islets were incubated (10 islets/well) for 30 min in Krebs-Ringer solution with either 3 mmol/L, 10mmol/L, 17mmol/L glucose, 20mmol/L KCl or 10mmol/L glucose

supplemented with 100nmol/L exendin-4 (Wuxi Apptec), the glucagon-like peptide-1 (GLP-1; Wuxi Apptect) or the glucose-dependent insulinotropic peptide (GIP; Wuxi Apptec). Secreted and total insulin content were quantified using a homogeneous time-resolved fluorescence (HTRF) insulin kit (Cisbio) in a PHERAstar reader (BMG Labtech), following the manufacturer's guidelines. Data are presented as secreted insulin/insulin content.

Single-cell fluorescence imaging Pancreatic islets were isolated from mice, dissociated into single β-cells and plated onto glass coverslips (Tarasov, Semplici et al. 2012). To study mitochondrial structure, cells were incubated with 100nM Mitotracker green (Thermo Fischer) in Krebs-Ringer bicarbonate buffer containing 11 mmol/L glucose for 30 min. Mitotracker green was then washed with Krebs buffer with 11 mmol/L glucose before fluorescence imaging. Single channel image stacks for Mitotracker green were recorded on a LSM780 inverted confocal microscope (Carl Zeiss, Cambridge, UK) using a ×63 1.4 numerical aperture (NA) oil objective and excitation with an argon laser (488 nm) and captured using a GaAsP (Carl Zeiss) detector. The image X,Y and Z dimensions were optimised (Nyquist settings) prior to capture images to enable post processing by deconvolution using Huygens software (Scientific Volume Imaging).

For experiments with tetramethylrhodamine ethyl ester (TMRE), β-cells were loaded with 10 nmol/L TMRE in modified Krebs-Ringer bicarbonate buffer (140 mmol/L NaCl, 3.6 mmol/L KCl, 0.5 mmol/L NaH_2PO_4, 24 mmol/L $NaHCO_3$ [saturated with CO_2], 1.5 mmol/L $CaCl_2$, 0.5 mmol/L $MgSO_4$, 10 mmol/L HEPES and 3 mmol/L glucose; pH 7.4) with 3 mmol/L glucose for 45 min and re-equilibrated with 2 nmol/L TMRE for 10 min

before recordings. TMRE (2 nmol/L) was present throughout and fluorescence was excited at 550 nm. Carbonyl cyanide-4-phenylhydrazone (FCCP; 1 μmol/L) was administrated, as indicated, and imaging was performed using an AxioObserver.Z1 microscope (Zeiss) using a ×40 1.4 NA oil objective, a CMOS ORCA Flash 4 camera (Hamamatsu) and a Colibri.2 light emitting diode (LED) excitation system (Zeiss; excitation filter 534/20 nm; emission filter 572/28 nm) at 0.3 Hz (250 ms exposure). Data were analysed using ImageJ (Schneider, Rasband et al. 2012). Traces represent mean normalised fluorescence intensity over time (F/F_{min}), where F_{min} is the mean fluorescence recorded during the application of 3 mmol/L glucose.

Mitochondrial shape analysis To determine morphological characteristics of mitochondria, confocal stacks were analysed with ImageJ using an in-house macro (available upon request). Briefly, for each stack, one image at the top, middle and bottom of the islet was analysed. After background subtraction, the following parameters were measured for each cell: number of particles, perimeter and circularity of each particle and elongation (1/circularity) was calculated (Wiemerslage and Lee 2016). The average perimeter, circularity and elongation of particles was then calculated for each cell.

Whole-islet fluorescence imaging Mitochondrial Ca^{2+} imaging of whole islets was performed after infection with adenovirus encoding the mitochondrially-targeted probe, R-GECO as previously described (Georgiadou, Haythorne et al. 2020) (Addgene; RRID:Addgene_46021; MOI: 100; [48 h post-isolation]) in modified Krebs-Ringer bicarbonate buffer. To examine ATP:ADP changes in response to a rise in extracellular glucose concentration, islets were infected as previously described

(Georgiadou, Haythorne et al. 2020) with an adenovirus bearing cDNA encoding the ATP sensor pGW1CMV-Perceval (RRID:Addgene_21737; MOI: 100; kindly provided by G. Yellen [Yale University, USA]) (Tarasov, Semplici et al. 2012) and incubated for 48 h prior to fluorescence imaging. Cytosolic Ca^{2+} imaging was performed after incubation with Cal-520 acetoxymethyl (AM; 2 µmol/L; 24 h post-isolation; Stratech) for 45 min in Krebs-Ringer bicarbonate buffer containing 3 mmol/L. Imaging was performed in Krebs supplemented with 3mmol/L or 17 mmol/L glucose, 17 mmol/L glucose with 0.1 mmol/L diazoxide (Diaz; Sigma-Aldrich), or 20 mmol/L KCl with diazoxide. ER Ca^{2+} storage was determined after incubation of islets with Cal-520 and 3 mmol/L glucose and imaged in Krebs buffer supplemented with 3 mmol/L or 17 mmol/L glucose, 17 mmol/L glucose with 0.1 mmol/L diazoxide or 100µmol/L acethyl choline (Sigma). All images were captured at 0.5 Hz on a Zeiss Axiovert microscope equipped with a ×10 0.5 NA objective, a Hamamatsu image-EM camera coupled to a Nipkow spinning-disk head (Yokogawa CSU-10) and illuminated at 490 nm (Cal-520, Perceval) or 580 nm (R-GECO). Data were analysed using ImageJ (W.S 1997-2018).

TIRF fluorescence imaging For experiments using the membrane-located zinc sensor ZIMIR (Li, Chen et al. 2011) islets from WT and KO islets were dissociated using accutase at 37°C during 5 min and dissociated cells were left to attach on a poly-L-lysine treated glass slides for 3 hours before incubation in KREBS buffer containing 3 mmol/L glucose and ZIMIR (50 µmol/L) for 40 min. Live-imaging at the membrane was performed on a Nikon Ti microscope equipped with a iLas2 TIRF module and a 100x/1.49 TIRF objective at 488 nM excitation. Acquisition rate was 3 images/second and after 3 min, KCl was added to a final concentration of 20 mmol/L.

For experiments using the fluorescent genetically-encoded and vesicle-located green marker NPY-Venus, islets were infected with an NPY-Venus adenoviral construct (Tsuboi and Rutter 2003) and left for expression for 48 hours. Islets were then dissociated as described above, left to attach to glass slide and fixed using 4% PFA in PBS. TIRF imaging was performed using the same microscopy system.

Pancreas immunohistochemistry Isolated pancreata were fixed in 4% (vol/vol) buffered formalin and embedded in paraffin wax within 24 h of removal. Slides (5 µm) were submerged sequentially in Histoclear (Sigma, UK) followed by washing in decreasing concentrations of ethanol to remove paraffin wax. Permeabilised pancreatic slices were blotted with anti-guinea pig insulin (Cell Signalling; 1:500; #4590, RRID:AB_659820) and anti-mouse glucagon (Sigma; 1:1 000; G2654, RRID:AB_259852) primary antibodies. Slides were visualised by subsequent incubation with Alexa Fluor 488 and 568-labelled goat anti-guinea pig and anti-mouse antibodies (Thermo Fischer; 1:1 000; #A-11073, RRID:AB_2534117 and #A-11004, RRID:AB_2534072). For examination of apoptosis, TUNEL assay was performed using a DeadEnd Fluorometric TUNEL system kit and DNase I treatment (Promega) according to the manufacturer's instructions. Samples were mounted on glass slides using Vectashield™ (Vector Laboratories) containing DAPI. Images were captured on a Zeiss AxioObserver.Z1 microscope using a ×40 Plan-Apochromat 206/0.8 M27 air objective, a CMOS ORCA Flash 4 camera (Hamamatsu) with a Colibri.2 LED illumination system. Fluorescent quantification was achieved using ImageJ with a purpose-designed macro (available upon request). Whole pancreas sections were used to quantitate cell mass. The number of TUNEL-positive cells of all visible islets was measured using ImageJ.

Metabolomics/lipidomics One method measuring mouse plasma molecules focused on a panel of known metabolites previously associated with diabetes, diabetes complications and metabolic dysfunction. These molecules were fully quantified using targeted ultra-high-performance liquid-chromatography coupled triple quadrupole mass spectrometry (UHPLC-QqQ-MS/MS) as described earlier (Ahonen, Jäntti et al. 2019). The second method aimed to measure a broad array of lipid species. Lipidomic sample preparation followed the Folch procedure with minor adjustments (Folch, Lees et al. 1957). Lipids were measured with ultra-high-performance liquid-chromatography coupled quadruple-time-of-flight mass spectrometry (UHPLC-QTOF/MS) in both positive and negative ionization mode, identification was done using MZmine (version 2.28) matching to an in-house library (Pluskal, Castillo et al. 2010). Peak areas were normalized to internal standards (Whiley, Godzien et al. 2012). Significance was tested by Student's two-tailed t-test using GraphPad Prism 8 software.

Measurement of oxygen consumption rate Seahorse XF96 extracellular flux analyzer (Seahorse Bioscience) was used for intact mouse islets respirometry. For XF96 assays, mouse islets (~10 per well) were seeded in 1µL/well Matrigel (Corning) in a poly-D-lysine (PDL)-coated XF96 plate and size-matched between conditions. Islets were incubated at 37 °C for 3.5min to solidify the Matrigel before the addition of 150µL/well of Seahorse assay media (XF Base Media Minimal DMEM, pH 7.4 supplemented with 3mmol/L glucose, 200mM L-glutamine, 100mM sodium pyruvate and 0.1% FBS). Islets were incubated at 37 °C for approximately 1hr before starting the assay. 4 baseline (under 3mmol/L glucose) OCR measurements were taken before the following substrates/compounds were injected: 20mmol/L glucose in port

A, followed by Oligomycin (Sigma, final concentration of 5µM) in port B, FCCP (Sigma, final concentration of 1µM FCCP) in port C, and Antimycin A with Rotenone (Sigma, final concentration of 5µM) in port D. Data are presented as either pmol O_2/min/islets.

Electron microscopy (EM) For conventional EM, islets were chemically fixed in 2% paraformaldehyde (EM grade, TAAB Laboratories Equipment), 2% glutaraldehyde and 3 mM $CaCl_2$ in 0.1 M cacodylate buffer (Sigma) for 2 h at room temperature then left overnight at 4°C in fresh fixative solution, osmicated, enrobed in agarose plugs, dehydrated in ethanol and embedded on Epon (TAAB Laboratories Equipment). Epon was polymerised overnight at 60°C. Ultrathin 70 nm sections were cut with a diamond knife (DiATOME) in a Ultracut UCT ultramicrotome (Leica) before examination on a Tecnai T12 TEM (FEI). Images were acquired in a charge-coupled device camera (Eagle), and processed in ImageJ.

***In vivo* Ca^{2+} imaging of AAV8-INS-GCaMP6s infected endogenous pancreatic islets** All mice were i.p. injected with tamoxifen daily at 15 weeks old. Endogenous pancreatic islets of WT and β*Mfn1/2*-KO mice (16 weeks old) were then infected with AAV8-INS-GCaMP6s (Reissaus, Piñeros et al. 2019) viral particles ($1*10^{14}$ or $10.1*10^{13}$ genome copies/ml) via i.p. injection (50µl/mouse), 24-28 days prior to terminal intravital imaging. On the day of imaging, mice were anesthetized with 2-4% inhaled isoflurane, the pancreas was then externalised and placed on a coverslip on a TCS SP8 DIVE (Leica) multiphoton platform equipped with heating pads and an objective warmer. Heated blankets were used at all times and temperature was constantly monitored using a rodent rectal temperature probe throughout the imaging session. A ×40 1.1 NA water immersion objective was used during imaging. Islets were

identified using green fluorescence from the GCaMP6s biosensor. Dyes suspended in saline, including Hoechst 33342 (Thermo Fisher Scientific: H3570; 70μg), tetramethylrhodamine methyl ester (TMRM, Thermo Fisher Scientific T668; 3μg) and Alexa Fluor 647 NHS Ester (Thermo Fisher Scientific; A20006) conjugated to Rat serum Albumin (Albumin-647; 500μg) were injected retro-orbitally to label nuclei, mitochondria and vasculature, respectively. *In vivo* Ca^{2+} imaging was performed by simultaneously exciting GCaMP6s at both 820 nm and 940 nm to capture non-excited and excited states of Ca^{2+} activity in the β-cells. Fluorescent emission was detected by an external HyD detector (Leica) through a 500-550 nm bandpass filter. Hoechst, TMRM and the dual excitable Albumin-647 were excited at 820 nm and fluorescence emission was detected by either external PMT (Leica) or HyD detectors through 400-470 nm, 570-630 nm and 650-750 nm bandpass filters, respectively. Baseline imaging of islets were recorded 10 min prior i.p. injection of glucose (1g/kg in sterile saline). The same islets were imaged for ~20 min to monitor Ca^{2+} oscillations post glucose injection. Baseline and post-imaging glucose measurements were obtained using an AlphaTRAK 2 glucometer. All images were collected at a scan speed of 600 Hz with a line average of 2, and a 512 x 512 frame size, with a frame rate of 0.576/s. At the end of each imaging session, animals were perfused with 4% (vol/vol) PFA and tissues were paraffin-embedded for further analysis. All *in vivo* imaging experiments were performed with approval and oversight from the Indiana University Institutional Animal Care and Use Committee (IACUC).

Fluorescent traces were calibrated to calculate fluorescence spikes fold change above the baseline on three cells per condition using ImageJ. Then the AUC was determined, with a threshold at 0.15 to subtract background noise.

Monte Carlo-based signal binarisation and data shuffling for identification of highly connected cells Data were analysed using approaches similar to those previously described (Johnston, Mitchell et al. 2016, Salem, Silva et al. 2019). Ca^{2+} signals were denoised by subjecting the signal the Huang-Hilbert type (HHT) empirical mode decomposition (EMD). The signals were decomposed into their intrinsic mode functions (IMFs) in MATLAB (MathWorks) (Flandrin 2008). The residual and the first IMF with the high-frequency components were then rejected to remove random noise. The Hilbert-Huang Transform was then performed to retrieve the instantaneous frequencies (Huang , HUANG, WU et al. 2009, Shen 2014) of the other IMFs to reconstruct the new signal using

$$X(t) = Re\sum_{j=1}^{N} a_j(t)e^{i\int \omega_j(t)dt}$$

where $a_j(t)$ = amplitude, $\omega_j(t)$ = frequency of the *i*th IMF component to retrieve a baseline trend and to account for any photobleaching or movement artefacts. A 20% threshold was imposed to minimise false positives from any residual fluctuations in baseline fluorescence.

Cell signals with deflection above the de-trended baseline were represented as '1' and inactivity represented as '0', thus binarising the signal at each time point. The coactivity of every cell pair was then measured as:

$$C_{ij} = \frac{T_{ij}}{\sqrt{T_i T_j}}$$

where T_{ij} = total coactivity time, T_i and T_j = total activity time for two cells.

The significance at $p<0.001$ of each coactivity measured against chance was assessed by subjecting the activity events of each cell to a Monte Carlo simulation (Björnsdotter, Rylander et al. 2011, Shultis 2011) with 10,000 iterations.

Synchronised Ca^{2+}-spiking behaviour was assessed by calculating the percentage of coactivity using the binarised cell activity dataset. A topographic representation of the connectivity was plotted in MATLAB with the edge colours representing the strength of the coactivity between any two cells.

An 80% threshold was imposed to determine the probability of the data, which was then plotted as a function of the number of connections for each cell to determine if the dataset obeyed a power-law relationship (Hodson, Molino et al. 2010).

RNA-Seq data analysis Processing and differential expression analysis of RNA-Seq data from high fat high sugar (HFHS) and regular chow (RC) fed mice was performed previously (Cruciani-Guglielmacci, Bellini et al. 2017). Briefly, differentially expressed genes were computed for the HFHS vs RC comparisons at 4 time-points for each of six mouse strains using the *Limma* package in R and p-values were adjusted for multiple comparisons using the Benjamini Hochberg procedure (Benjamini and Hochberg 1995).

Statistics Data are expressed as mean ± SEM unless otherwise stated. Significance was tested by Student's two-tailed t-test and Mann–Whitney correction or two-way ANOVA with Sidak's multiple comparison test for comparison of more than two groups, using GraphPad Prism 8 software. $p<0.05$ was considered significant.

Electronic Supplemental Tables

ESM Table 1. Sequence of primers used for genotyping *Mfn1* and *Mfn2* flox.

ESM Table 2. List of primers used for qRT-PCR.

ESM Table 3. Metabolite differences found in plasma samples of WT vs KO mice according to metabolic class and both fold-change and t-test criteria.

References

Ahonen, L., S. Jäntti, T. Suvitaival, S. Theilade, C. Risz, R. Kostiainen, P. Rossing, M. Orešič and T. Hyötyläinen (2019). "Targeted Clinical Metabolite Profiling Platform for the Stratification of Diabetic Patients." Metabolites 9(9): 184.

Andersén, E., G. Karlaganis and J. Sjövall (1988). "Altered bile acid profiles in duodenal bile and urine in diabetic subjects." Eur J Clin Invest 18(2): 166-172.

Anderson, A. J., T. D. Jackson, D. A. Stroud and D. Stojanovski (2019). "Mitochondria-hubs for regulating cellular biochemistry: emerging concepts and networks." Open biology 9(8): 190126-190126.

Anello, M., R. Lupi, D. Spampinato, S. Piro, M. Masini, U. Boggi, S. Del Prato, A. M. Rabuazzo, F. Purrello and P. Marchetti (2005). "Functional and morphological alterations of mitochondria in pancreatic beta cells from type 2 diabetic patients." Diabetologia 48(2): 282-289.

Araki, E., S. Oyadomari and M. Mori (2003). "Impact of Endoplasmic Reticulum Stress Pathway on Pancreatic β-Cells and Diabetes Mellitus." Experimental Biology and Medicine 228(10): 1213-1217.

Ashcroft, F. M. and P. Rorsman (2013). "K(ATP) channels and islet hormone secretion: new insights and controversies." Nat Rev Endocrinol 9(11): 660-669.

Bach, D., D. Naon, S. Pich, F. X. Soriano, N. Vega, J. Rieusset, M. Laville, C. Guillet, Y. Boirie, H. Wallberg-Henriksson, M. Manco, M. Calvani, M. Castagneto, M. Palacin, G. Mingrone, J. R. Zierath, H. Vidal and A. Zorzano (2005). "Expression of Mfn2, the Charcot-Marie-Tooth neuropathy type 2A gene, in human skeletal muscle: effects of type 2 diabetes, obesity, weight loss, and the regulatory role of tumor necrosis factor alpha and interleukin-6." Diabetes 54(9): 2685-2693.

Bach, D., S. Pich, F. X. Soriano, N. Vega, B. Baumgartner, J. Oriola, J. R. Daugaard, J. Lloberas, M. Camps, J. R. Zierath, R. Rabasa-Lhoret, H. Wallberg-Henriksson, M. Laville, M. Palacín, H. Vidal, F. Rivera, M. Brand and A. Zorzano (2003). "Mitofusin-2 Determines Mitochondrial Network Architecture and Mitochondrial Metabolism: a novel regulatory mechanism altered in obesity." Journal of Biological Chemistry 278(19): 17190-17197.

Benjamini, Y. and Y. Hochberg (1995). "Controlling the false discovery rate: a practical and powerful approach to multiple testing." Journal of the Royal Statistical Society Series B 57: 289–300.

Björnsdotter, M., K. Rylander and J. Wessberg (2011). "A Monte Carlo method for locally multivariate brain mapping." Neuroimage 56(2): 508-516.

Brereton, M. F., M. Iberl, K. Shimomura, Q. Zhang, A. E. Adriaenssens, P. Proks, Spiliotis, II, W. Dace, K. K. Mattis, R. Ramracheya, F. M. Gribble, F. Reimann, A. Clark, P. Rorsman and F. M. Ashcroft (2014). "Reversible changes in pancreatic islet structure and function produced by elevated blood glucose." Nat Commun 5: 4639.

Butler, A. E., J. Janson, S. Bonner-Weir, R. Ritzel, R. A. Rizza and P. C. Butler (2003). "Beta-cell deficit and increased beta-cell apoptosis in humans with type 2 diabetes." Diabetes 52(1): 102-110.

Chandhok, G., M. Lazarou and B. Neumann (2018). "Structure, function, and regulation of mitofusin-2 in health and disease." Biol Rev Camb Philos Soc 93(2): 933-949.

Chen, H., J. M. McCaffery and D. C. Chan (2007). "Mitochondrial fusion protects against neurodegeneration in the cerebellum." Cell 130(3): 548-562.

Cogliati, S., C. Frezza, M. E. Soriano, T. Varanita, R. Quintana-Cabrera, M. Corrado, S. Cipolat, V. Costa, A. Casarin, L. C. Gomes, E. Perales-Clemente, L. Salviati, P. Fernandez-Silva, J. A. Enriquez and L. Scorrano (2013). "Mitochondrial cristae shape determines

respiratory chain supercomplexes assembly and respiratory efficiency." Cell 155(1): 160-171.
Cruciani-Guglielmacci, C., L. Bellini, J. Denom, M. Oshima, N. Fernandez, P. Normandie-Levi, X. P. Berney, N. Kassis, C. Rouch, J. Dairou, T. Gorman, D. M. Smith, A. Marley, R. Liechti, D. Kuznetsov, L. Wigger, F. Burdet, A.-L. Lefèvre, I. Wehrle, I. Uphues, T. Hildebrandt, W. Rust, C. Bernard, A. Ktorza, G. A. Rutter, R. Scharfmann, I. Xenarios, H. Le Stunff, B. Thorens, C. Magnan and M. Ibberson (2017). "Molecular phenotyping of multiple mouse strains under metabolic challenge uncovers a role for Elovl2 in glucose-induced insulin secretion." Molecular Metabolism 6(4): 340-351.
Cruciani-Guglielmacci, C., L. Bellini, J. Denom, M. Oshima, N. Fernandez, P. Normandie-Levi, X. P. Berney, N. Kassis, C. Rouch, J. Dairou, T. Gorman, D. M. Smith, A. Marley, R. Liechti, D. Kuznetsov, L. Wigger, F. Burdet, A.-L. Lefèvre, I. Wehrle, I. Uphues, T. Hildebrandt, W. Rust, C. Bernard, A. Ktorza, G. A. Rutter, R. Scharfmann, I. Xenarios, H. Le Stunff, B. Thorens, C. Magnan and M. Ibberson (2017). "Molecular phenotyping of multiple mouse strains under metabolic challenge uncovers a role for Elovl2 in glucose-induced insulin secretion." Molecular Metabolism.
Del Guerra, S., R. Lupi, L. Marselli, M. Masini, M. Bugliani, S. Sbrana, S. Torri, M. Pollera, U. Boggi, F. Mosca, S. Del Prato and P. Marchetti (2005). "Functional and molecular defects of pancreatic islets in human type 2 diabetes." Diabetes 54(3): 727-735.
Dlaskova, A., T. Spacek, J. Santorova, L. Plecita-Hlavata, Z. Berkova, F. Saudek, M. Lessard, J. Bewersdorf and P. Jezek (2010). "4Pi microscopy reveals an impaired three-dimensional mitochondrial network of pancreatic islet beta-cells, an experimental model of type-2 diabetes." Biochim Biophys Acta 1797(6-7): 1327-1341.
Duran-Sandoval, D., G. Mautino, G. Martin, F. Percevault, O. Barbier, J.-C. Fruchart, F. Kuipers and B. Staels (2004). "Glucose Regulates the Expression of the Farnesoid X Receptor in Liver." Diabetes 53(4): 890-898.
Eisner, V., M. Picard and G. Hajnoczky (2018). "Mitochondrial dynamics in adaptive and maladaptive cellular stress responses." Nat Cell Biol 20(7): 755-765.
Elayat, A. A., M. M. el-Naggar and M. Tahir (1995). "An immunocytochemical and morphometric study of the rat pancreatic islets." J Anat 186 (Pt 3)(Pt 3): 629-637.
Filadi, R., E. Greotti, G. Turacchio, A. Luini, T. Pozzan and P. Pizzo (2017). "On the role of Mitofusin 2 in endoplasmic reticulum-mitochondria tethering." Proc Natl Acad Sci U S A 114(12): E2266-e2267.
Filadi, R., D. Pendin and P. Pizzo (2018). "Mitofusin 2: from functions to disease." Cell Death & Disease 9(3): 330.
Flandrin, G. R. a. P. (2008). "One or Two Frequencies? The Empirical Mode Decomposition Answers." IEEE Transactions on signal processing 56(1).
Folch, J., M. Lees and G. H. Sloane Stanley (1957). "A simple method for the isolation and purification of total lipides from animal tissues." J Biol Chem 226(1): 497-509.
Frank, S., B. Gaume, E. S. Bergmann-Leitner, W. W. Leitner, E. G. Robert, F. Catez, C. L. Smith and R. J. Youle (2001). "The role of dynamin-related protein 1, a mediator of mitochondrial fission, in apoptosis." Dev Cell 1(4): 515-525.
Gao, Y., F. Li, A. Zhang, L. Wang, W. Tong and B. Liu (2014). "Evaluation of mitochondrial divisions in mouse with type-2 diabetes and effect of glucose-oxidase on mouse islet cells RIN-m5F." Cell Biol Int 38(3): 368-373.
Gegg, M. E., J. M. Cooper, K. Y. Chau, M. Rojo, A. H. Schapira and J. W. Taanman (2010). "Mitofusin 1 and mitofusin 2 are ubiquitinated in a PINK1/parkin-dependent manner upon induction of mitophagy." Hum Mol Genet 19(24): 4861-4870.

Georgiadou, E., E. Haythorne, M. T. Dickerson, L. Lopez-Noriega, T. J. Pullen, G. da Silva Xavier, S. P. X. Davis, A. Martinez-Sanchez, F. Semplici, R. Rizzuto, J. A. McGinty, P. M. French, M. C. Cane, D. A. Jacobson, I. Leclerc and G. A. Rutter (2020). "The pore-forming subunit MCU of the mitochondrial Ca2+ uniporter is required for normal glucose-stimulated insulin secretion in vitro and in vivo in mice." Diabetologia 63(7): 1368-1381.
Gilon, P., H.-Y. Chae, G. A. Rutter and M. A. Ravier (2014). "Calcium signaling in pancreatic β-cells in health and in Type 2 diabetes." Cell Calcium 56(5): 340-361.
Gu, G., J. Dubauskaite and D. A. Melton (2002). "Direct evidence for the pancreatic lineage: NGN3+ cells are islet progenitors and are distinct from duct progenitors." Development 129(10): 2447-2457.
Hassan, A. S., M. T. R. Subbiah and P. Thiebert (1980). "Specific Changes of Bile Acid Metabolism in Spontaneously Diabetic Wistar Rats." Proceedings of the Society for Experimental Biology and Medicine 164(4): 449-452.
Haythorne, E., M. Rohm, M. van de Bunt, M. F. Brereton, A. I. Tarasov, T. S. Blacker, G. Sachse, M. Silva Dos Santos, R. Terron Exposito, S. Davis, O. Baba, R. Fischer, M. R. Duchen, P. Rorsman, J. I. MacRae and F. M. Ashcroft (2019). "Diabetes causes marked inhibition of mitochondrial metabolism in pancreatic β-cells." Nat Commun 10(1): 2474.
Heath-Engel, H. M. and G. C. Shore (2006). "Mitochondrial membrane dynamics, cristae remodelling and apoptosis." Biochim Biophys Acta 1763(5-6): 549-560.
Hennings, T. G., D. G. Chopra, E. R. DeLeon, H. R. VanDeusen, H. Sesaki, M. J. Merrins and G. M. Ku (2018). "In Vivo Deletion of beta-Cell Drp1 Impairs Insulin Secretion Without Affecting Islet Oxygen Consumption." Endocrinology 159(9): 3245-3256.
Henquin, J. C. (2000). "Triggering and amplifying pathways of regulation of insulin secretion by glucose." Diabetes 49(11): 1751-1760.
Higa, M., Y. T. Zhou, M. Ravazzola, D. Baetens, L. Orci and R. H. Unger (1999). "Troglitazone prevents mitochondrial alterations, beta cell destruction, and diabetes in obese prediabetic rats." Proc Natl Acad Sci U S A 96(20): 11513-11518.
Hodson, D. J., F. Molino, P. Fontanaud, X. Bonnefont and P. Mollard (2010). "Investigating and modelling pituitary endocrine network function." J Neuroendocrinol 22(12): 1217-1225.
Huang, N. E. Introduction to the hilbert–huang transform and its related mathematical problems. Hilbert-Huang Transform and Its Applications: 1-26.
Huang, N. E., Z. Wu, S. R. Long, K. C. Arnold, X. Chen And K. Blank (2009). "on instantaneous frequency." Advances in Adaptive Data Analysis 01(02): 177-229.
Hwa, J. J., M. A. Hiller, M. T. Fuller and A. Santel (2002). "Differential expression of the Drosophila mitofusin genes fuzzy onions (fzo) and dmfn." Mech Dev 116(1-2): 213-216.
Johnston, N. R., R. K. Mitchell, E. Haythorne, M. P. Pessoa, F. Semplici, J. Ferrer, L. Piemonti, P. Marchetti, M. Bugliani, D. Bosco, E. Berishvili, P. Duncanson, M. Watkinson, J. Broichhagen, D. Trauner, G. A. Rutter and D. J. Hodson (2016). "Beta Cell Hubs Dictate Pancreatic Islet Responses to Glucose." Cell Metab 24(3): 389-401.
Khan, R., A. Tomas and G. A. Rutter (2020). "Effects on pancreatic Beta and other Islet cells of the glucose-dependent insulinotropic polypeptide." Peptides 125: 170201.
Kolesar, J. E., C. Y. Wang, Y. V. Taguchi, S. H. Chou and B. A. Kaufman (2013). "Two-dimensional intact mitochondrial DNA agarose electrophoresis reveals the structural complexity of the mammalian mitochondrial genome." Nucleic Acids Res 41(4): e58.
Komatsu, M., S. Waguri, M. Koike, Y. S. Sou, T. Ueno, T. Hara, N. Mizushima, J. Iwata, J. Ezaki, S. Murata, J. Hamazaki, Y. Nishito, S. Iemura, T. Natsume, T. Yanagawa, J. Uwayama, E. Warabi, H. Yoshida, T. Ishii, A. Kobayashi, M. Yamamoto, Z. Yue, Y.

Uchiyama, E. Kominami and K. Tanaka (2007). "Homeostatic levels of p62 control cytoplasmic inclusion body formation in autophagy-deficient mice." Cell 131(6): 1149-1163.
Kone, M., T. J. Pullen, G. Sun, M. Ibberson, A. Martinez-Sanchez, S. Sayers, M. S. Nguyen-Tu, C. Kantor, A. Swisa, Y. Dor, T. Gorman, J. Ferrer, B. Thorens, F. Reimann, F. Gribble, J. A. McGinty, L. Chen, P. M. French, F. Birzele, T. Hildebrandt, I. Uphues and G. A. Rutter (2014). "LKB1 and AMPK differentially regulate pancreatic beta-cell identity." Faseb j 28(11): 4972-4985.
Kwon, G., C. A. Marshall, K. L. Pappan, M. S. Remedi and M. L. McDaniel (2004). "Signaling elements involved in the metabolic regulation of mTOR by nutrients, incretins, and growth factors in islets." Diabetes 53 Suppl 3: S225-232.
Lamichhane, S., L. Ahonen, T. S. Dyrlund, E. Kemppainen, H. Siljander, H. Hyöty, J. Ilonen, J. Toppari, R. Veijola, T. Hyötyläinen, M. Knip and M. Oresic (2018). "Dynamics of Plasma Lipidome in Progression to Islet Autoimmunity and Type 1 Diabetes - Type 1 Diabetes Prediction and Prevention Study (DIPP)." Scientific reports 8(1): 10635-10635.
Li, D., S. Chen, E. A. Bellomo, A. I. Tarasov, C. Kaut, G. A. Rutter and W. H. Li (2011). "Imaging dynamic insulin release using a fluorescent zinc indicator for monitoring induced exocytotic release (ZIMIR)." Proc Natl Acad Sci U S A 108(52): 21063-21068.
Liesa, M. and O. S. Shirihai (2013). "Mitochondrial dynamics in the regulation of nutrient utilization and energy expenditure." Cell Metab 17(4): 491-506.
Lowell, B. B. and G. I. Shulman (2005). "Mitochondrial dysfunction and type 2 diabetes." Science 307(5708): 384-387.
Maechler, P. and C. B. Wollheim (2001). "Mitochondrial function in normal and diabetic beta-cells." Nature 414(6865): 807-812.
Maldonado, E. N., K. L. Sheldon, D. N. DeHart, J. Patnaik, Y. Manevich, D. M. Townsend, S. M. Bezrukov, T. K. Rostovtseva and J. J. Lemasters (2013). "Voltage-dependent anion channels modulate mitochondrial metabolism in cancer cells: regulation by free tubulin and erastin." The Journal of biological chemistry 288(17): 11920-11929.
Marchetti, P., S. Del Guerra, L. Marselli, R. Lupi, M. Masini, M. Pollera, M. Bugliani, U. Boggi, F. Vistoli, F. Mosca and S. Del Prato (2004). "Pancreatic islets from type 2 diabetic patients have functional defects and increased apoptosis that are ameliorated by metformin." J Clin Endocrinol Metab 89(11): 5535-5541.
Masini, M., L. Martino, L. Marselli, M. Bugliani, U. Boggi, F. Filipponi, P. Marchetti and V. De Tata (2017). "Ultrastructural alterations of pancreatic beta cells in human diabetes mellitus." Diabetes/Metabolism Research and Reviews 33(6): e2894.
McCormack, J. G., A. P. Halestrap and R. M. Denton (1990). "Role of calcium ions in regulation of mammalian intramitochondrial metabolism." Physiol Rev 70(2): 391-425.
McDaniel, M. L., C. A. Marshall, K. L. Pappan and G. Kwon (2002). "Metabolic and autocrine regulation of the mammalian target of rapamycin by pancreatic beta-cells." Diabetes 51(10): 2877-2885.
Molina, A. J. A., J. D. Wikstrom, L. Stiles, G. Las, H. Mohamed, A. Elorza, G. Walzer, G. Twig, S. Katz, B. E. Corkey and O. S. Shirihai (2009). "Mitochondrial networking protects beta-cells from nutrient-induced apoptosis." Diabetes 58(10): 2303-2315.
Mulder, H. and C. Ling (2009). "Mitochondrial dysfunction in pancreatic beta-cells in Type 2 diabetes." Mol Cell Endocrinol 297(1-2): 34-40.
Nauck, M. A. and J. J. Meier (2018). "Incretin hormones: Their role in health and disease." Diabetes, Obesity and Metabolism 20(S1): 5-21.

Olichon, A., L. Baricault, N. Gas, E. Guillou, A. Valette, P. Belenguer and G. Lenaers (2003). "Loss of OPA1 perturbates the mitochondrial inner membrane structure and integrity, leading to cytochrome c release and apoptosis." J Biol Chem 278(10): 7743-7746.
Paltauf-Doburzynska, J., R. Malli and W. F. Graier (2004). "Hyperglycemic conditions affect shape and Ca2+ homeostasis of mitochondria in endothelial cells." J Cardiovasc Pharmacol 44(4): 423-436.
Panten, U. and H. Ishida (1974). "Proceedings: Flavin fluorescence of isolated pancreatic islets." Naunyn Schmiedebergs Arch Pharmacol 282(Suppl): suppl 282:R273.
Pipeleers, D., P. I. in't Veld, E. Maes and M. Van De Winkel (1982). "Glucose-induced insulin release depends on functional cooperation between islet cells." Proc Natl Acad Sci U S A 79(23): 7322-7325.
Pluskal, T., S. Castillo, A. Villar-Briones and M. Oresic (2010). "MZmine 2: modular framework for processing, visualizing, and analyzing mass spectrometry-based molecular profile data." BMC Bioinformatics 11: 395.
Pullen, T. J., M. O. Huising and G. A. Rutter (2017). "Analysis of Purified Pancreatic Islet Beta and Alpha Cell Transcriptomes Reveals 11β-Hydroxysteroid Dehydrogenase (Hsd11b1) as a Novel Disallowed Gene." Front Genet 8: 41.
Quintana-Cabrera, R., A. Mehrotra, G. Rigoni and M. E. Soriano (2018). "Who and how in the regulation of mitochondrial cristae shape and function." Biochemical and Biophysical Research Communications 500(1): 94-101.
Quiros, P. M., A. J. Ramsay, D. Sala, E. Fernandez-Vizarra, F. Rodriguez, J. R. Peinado, M. S. Fernandez-Garcia, J. A. Vega, J. A. Enriquez, A. Zorzano and C. Lopez-Otin (2012). "Loss of mitochondrial protease OMA1 alters processing of the GTPase OPA1 and causes obesity and defective thermogenesis in mice." Embo j 31(9): 2117-2133.
Ravier, M. A. and G. A. Rutter (2010). "Isolation and culture of mouse pancreatic islets for ex vivo imaging studies with trappable or recombinant fluorescent probes." Methods Mol Biol 633: 171-184.
Reina, S., F. Guarino, A. Magrì and V. De Pinto (2016). "VDAC3 As a Potential Marker of Mitochondrial Status Is Involved in Cancer and Pathology." Frontiers in oncology 6: 264-264.
Reinhardt, F., J. Schultz, R. Waterstradt and S. Baltrusch (2016). "Drp1 guarding of the mitochondrial network is important for glucose-stimulated insulin secretion in pancreatic beta cells." Biochem Biophys Res Commun 474(4): 646-651.
Reissaus, C. A., A. R. Piñeros, A. N. Twigg, K. S. Orr, A. M. Conteh, M. M. Martinez, M. M. Kamocka, R. N. Day, S. A. Tersey, R. G. Mirmira, K. W. Dunn and A. K. Linnemann (2019). "A Versatile, Portable Intravital Microscopy Platform for Studying Beta-cell Biology In Vivo." Scientific Reports 9(1): 8449.
Rorsman, P. and F. M. Ashcroft (2018). "Pancreatic β-Cell Electrical Activity and Insulin Secretion: Of Mice and Men." Physiol Rev 98(1): 117-214.
Rovira-Llopis, S., C. Banuls, N. Diaz-Morales, A. Hernandez-Mijares, M. Rocha and V. M. Victor (2017). "Mitochondrial dynamics in type 2 diabetes: Pathophysiological implications." Redox Biol 11: 637-645.
Rui, J., S. Deng, A. Arazi, A. L. Perdigoto, Z. Liu and K. C. Herold (2017). "β Cells that Resist Immunological Attack Develop during Progression of Autoimmune Diabetes in NOD Mice." Cell Metab 25(3): 727-738.
Rutter GA, Georgiadou E, M.-S. A. and and P. TJ (2020). "Metabolic and functional specialisations of the pancreatic beta cell: gene disallowance, mitochondrial metabolism and intercellular connectivity." Diabetologia under review.

Rutter, G. A., E. Georgiadou, A. Martinez-Sanchez and T. J. Pullen (2020). "Metabolic and functional specialisations of the pancreatic beta cell: gene disallowance, mitochondrial metabolism and intercellular connectivity." Diabetologia 63(10): 1990-1998.
Rutter, G. A., T. J. Pullen, D. J. Hodson and A. Martinez-Sanchez (2015). "Pancreatic β-cell identity, glucose sensing and the control of insulin secretion." Biochem J 466(2): 203-218.
Rutter, G. A. and R. Rizzuto (2000). "Regulation of mitochondrial metabolism by ER Ca2+ release: an intimate connection." Trends in Biochemical Sciences 25(5): 215-221.
Salem, V., L. D. Silva, K. Suba, E. Georgiadou, S. Neda Mousavy Gharavy, N. Akhtar, A. Martin-Alonso, D. C. A. Gaboriau, S. M. Rothery, T. Stylianides, G. Carrat, T. J. Pullen, S. P. Singh, D. J. Hodson, I. Leclerc, A. M. J. Shapiro, P. Marchetti, L. J. B. Briant, W. Distaso, N. Ninov and G. A. Rutter (2019). "Leader β-cells coordinate Ca2+ dynamics across pancreatic islets in vivo." Nature Metabolism 1(6): 615-629.
Schneider, C. A., W. S. Rasband and K. W. Eliceiri (2012). "NIH Image to ImageJ: 25 years of image analysis." Nat Methods 9(7): 671-675.
Schrepfer, E. and L. Scorrano (2016). "Mitofusins, from Mitochondria to Metabolism." Mol Cell 61(5): 683-694.
Sebastian, D., M. I. Hernandez-Alvarez, J. Segales, E. Sorianello, J. P. Munoz, D. Sala, A. Waget, M. Liesa, J. C. Paz, P. Gopalacharyulu, M. Oresic, S. Pich, R. Burcelin, M. Palacin and A. Zorzano (2012). "Mitofusin 2 (Mfn2) links mitochondrial and endoplasmic reticulum function with insulin signaling and is essential for normal glucose homeostasis." Proc Natl Acad Sci U S A 109(14): 5523-5528.
Serasinghe, M. N. and J. E. Chipuk (2017). "Mitochondrial Fission in Human Diseases." Handb Exp Pharmacol 240: 159-188.
Shen, N. E. H. a. S. S. (2014). Hilbert–Huang Transform and Its Applications.
Shultis, W. D. a. J. K. (2011). Exploring Monte Carlo Methods.
Sidarala, V., G. L. Pearson, V. S. Parekh, B. Thompson, L. Christen, M. A. Gingerich, J. Zhu, T. Stromer, J. Ren, E. C. Reck, B. Chai, J. A. Corbett, T. Mandrup-Poulsen, L. S. Satin and S. A. Soleimanpour (2020). "Mitophagy protects beta cells from inflammatory damage in diabetes." JCI Insight.
Silva, J. P., M. Köhler, C. Graff, A. Oldfors, M. A. Magnuson, P.-O. Berggren and N.-G. Larsson (2000). "Impaired insulin secretion and β-cell loss in tissue-specific knockout mice with mitochondrial diabetes." Nature Genetics 26(3): 336-340.
Song, B., D. Scheuner, D. Ron, S. Pennathur and R. J. Kaufman (2008). "Chop deletion reduces oxidative stress, improves β cell function, and promotes cell survival in multiple mouse models of diabetes." The Journal of Clinical Investigation 118(10): 3378-3389.
Sorensen, C. M., J. Ding, Q. Zhang, T. Alquier, R. Zhao, P. W. Mueller, R. D. Smith and T. O. Metz (2010). "Perturbations in the lipid profile of individuals with newly diagnosed type 1 diabetes mellitus: lipidomics analysis of a Diabetes Antibody Standardization Program sample subset." Clinical biochemistry 43(12): 948-956.
Staels, B. and V. A. Fonseca (2009). "Bile Acids and Metabolic Regulation." Mechanisms and clinical responses to bile acid sequestration 32(suppl 2): S237-S245.
Stiles, L. and O. S. Shirihai (2012). "Mitochondrial dynamics and morphology in beta-cells." Best Pract Res Clin Endocrinol Metab 26(6): 725-738.
Supale, S., N. Li, T. Brun and P. Maechler (2012). "Mitochondrial dysfunction in pancreatic beta cells." Trends Endocrinol Metab 23(9): 477-487.
Szendroedi, J., E. Phielix and M. Roden (2012). "The role of mitochondria in insulin resistance and type 2 diabetes mellitus." Nature Reviews Endocrinology 8(2): 92-103.

Talchai, C., S. Xuan, H. V. Lin, L. Sussel and D. Accili (2012). "Pancreatic β cell dedifferentiation as a mechanism of diabetic β cell failure." Cell 150(6): 1223-1234.
Tanida, I. and S. Waguri (2010). Measurement of Autophagy in Cells and Tissues. Protein Misfolding and Cellular Stress in Disease and Aging: Concepts and Protocols. P. Bross and N. Gregersen. Totowa, NJ, Humana Press: 193-214.
Tarasov, A. I. and G. A. Rutter (2014). "Use of genetically encoded sensors to monitor cytosolic ATP/ADP ratio in living cells." Methods Enzymol 542: 289-311.
Tarasov, A. I., F. Semplici, M. A. Ravier, E. A. Bellomo, T. J. Pullen, P. Gilon, I. Sekler, R. Rizzuto and G. A. Rutter (2012). "The mitochondrial Ca2+ uniporter MCU is essential for glucose-induced ATP increases in pancreatic beta-cells." PLoS One 7(7): e39722.
Tarasov, A. I., F. Semplici, M. A. Ravier, E. A. Bellomo, T. J. Pullen, P. Gilon, I. Sekler, R. Rizzuto and G. A. Rutter (2012). "The Mitochondrial Ca2+ Uniporter MCU Is Essential for Glucose-Induced ATP Increases in Pancreatic β-Cells." PLOS ONE 7(7): e39722.
Tsuboi, T. and G. A. Rutter (2003). "Multiple forms of "kiss-and-run" exocytosis revealed by evanescent wave microscopy." Curr Biol 13(7): 563-567.
van den Ouweland, J. M., P. Maechler, C. B. Wollheim, G. Attardi and J. A. Maassen (1999). "Functional and morphological abnormalities of mitochondria harbouring the tRNA(Leu)(UUR) mutation in mitochondrial DNA derived from patients with maternally inherited diabetes and deafness (MIDD) and progressive kidney disease." Diabetologia 42(4): 485-492.
W.S, R. (1997-2018). "ImageJ, U. S. National Institutes of Health, Bethesda, Maryland, USA."
Wada, J. and A. Nakatsuka (2016). "Mitochondrial Dynamics and Mitochondrial Dysfunction in Diabetes." Acta Med Okayama 70(3): 151-158.
Wai, T. and T. Langer (2016). "Mitochondrial Dynamics and Metabolic Regulation." Trends Endocrinol Metab 27(2): 105-117.
Wang, L., T. Ishihara, Y. Ibayashi, K. Tatsushima, D. Setoyama, Y. Hanada, Y. Takeichi, S. Sakamoto, S. Yokota, K. Mihara, D. Kang, N. Ishihara, R. Takayanagi and M. Nomura (2015). "Disruption of mitochondrial fission in the liver protects mice from diet-induced obesity and metabolic deterioration." Diabetologia 58(10): 2371-2380.
Westermann, B. (2012). "Bioenergetic role of mitochondrial fusion and fission." Biochim Biophys Acta 1817(10): 1833-1838.
Whiley, L., J. Godzien, F. J. Ruperez, C. Legido-Quigley and C. Barbas (2012). "In-vial dual extraction for direct LC-MS analysis of plasma for comprehensive and highly reproducible metabolic fingerprinting." Anal Chem 84(14): 5992-5999.
Wiemerslage, L. and D. Lee (2016). "Quantification of mitochondrial morphology in neurites of dopaminergic neurons using multiple parameters." J Neurosci Methods 262: 56-65.
Yang, J., Y. Chi, B. R. Burkhardt, Y. Guan and B. A. Wolf (2010). "Leucine metabolism in regulation of insulin secretion from pancreatic beta cells." Nutrition reviews 68(5): 270-279.
Yin, Q., Q. Ni, Y. Wang, H. Zhang, W. Li, A. Nie, S. Wang, Y. Gu, Q. Wang and G. Ning (2020). "Raptor determines β-cell identity and plasticity independent of hyperglycemia in mice." Nature Communications 11(1): 2538.
Yisang Yoon, C. A. G., Bong Sook Jhun, and Tianzheng Yu (2011). "Mitochondrial Dynamics in Diabetes." Antioxidants & Redox Signaling 14(3): 439-457.
Yu, T., J. L. Robotham and Y. Yoon (2006). "Increased production of reactive oxygen species in hyperglycemic conditions requires dynamic change of mitochondrial morphology." Proc Natl Acad Sci U S A 103(8): 2653-2658.

Zhang, Z., N. Wakabayashi, J. Wakabayashi, Y. Tamura, W. J. Song, S. Sereda, P. Clerc, B. M. Polster, S. M. Aja, M. V. Pletnikov, T. W. Kensler, O. S. Shirihai, M. Iijima, M. A. Hussain and H. Sesaki (2011). "The dynamin-related GTPase Opa1 is required for glucose-stimulated ATP production in pancreatic beta cells." Mol Biol Cell 22(13): 2235-2245.
Zorzano, A., M. Liesa and M. Palacin (2009). "Mitochondrial dynamics as a bridge between mitochondrial dysfunction and insulin resistance." Arch Physiol Biochem 115(1): 1-12.

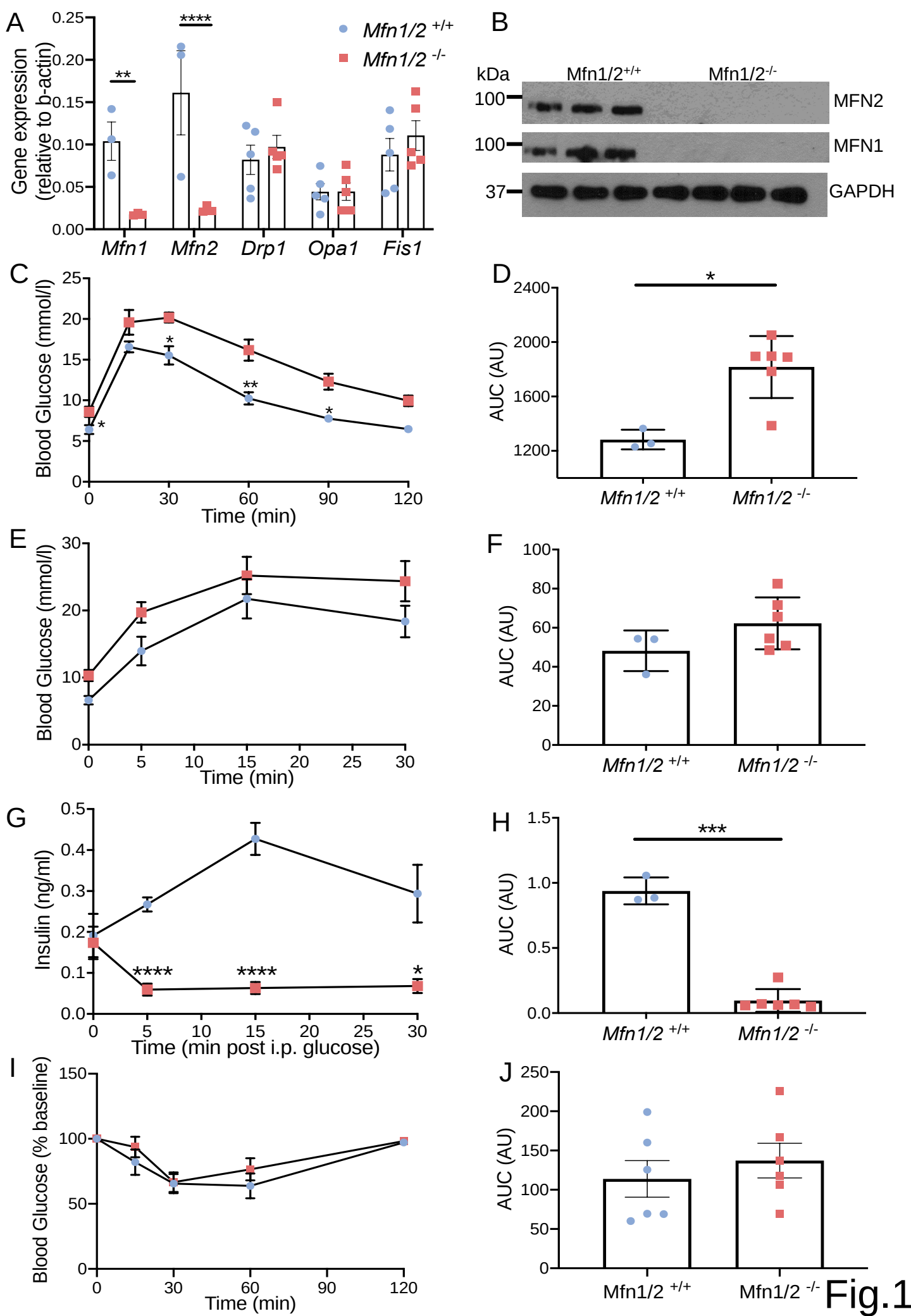
A
Gene expression (relative to b-actin)
Mfn1/2 +/+
Mfn1/2 -/-
**
****
Mfn1
Mfn2
Drp1
Opa1
Fis1
B
kDa
Mfn1/2+/+
Mfn1/2-/-
100
100
37
MFN2
MFN1
GAPDH
C
Blood Glucose (mmol/l)
Time (min)
D
AUC (AU)
*
Mfn1/2 +/+
Mfn1/2 -/-
E
Blood Glucose (mmol/l)
Time (min)
F
AUC (AU)
Mfn1/2 +/+
Mfn1/2 -/-
G
Insulin (ng/ml)
****
****
*
Time (min post i.p. glucose)
H
AUC (AU)
***
Mfn1/2 +/+
Mfn1/2 -/-
I
Blood Glucose (% baseline)
Time (min)
J
AUC (AU)
Mfn1/2 +/+
Mfn1/2 -/-

Fig.1

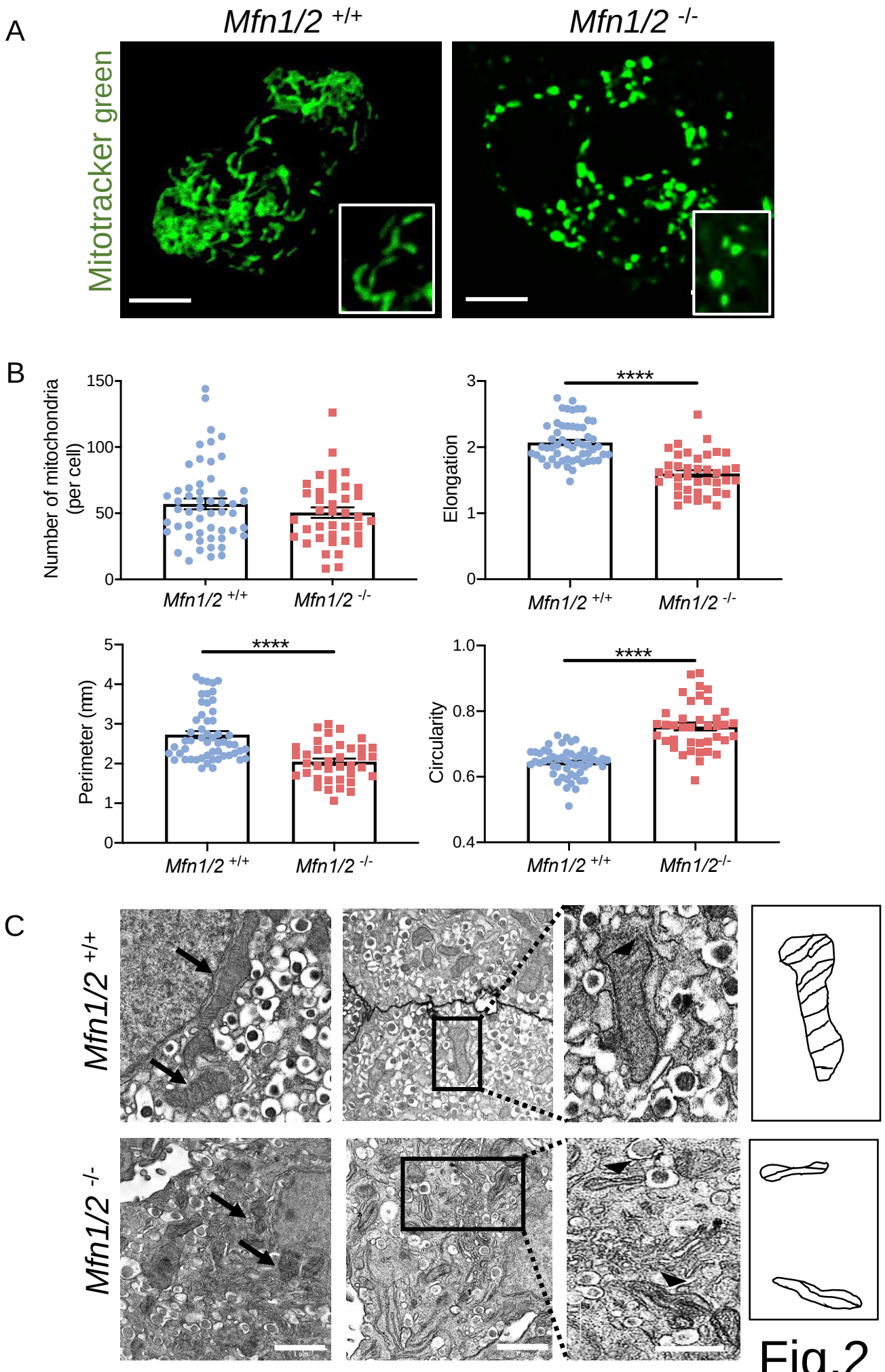
A
Mfn1/2 +/+
Mfn1/2 -/-
Mitotracker green
B
Number of mitochondria (per cell)
150
100
50
0
Mfn1/2 +/+
Mfn1/2 -/-
Elongation
****
3
2
1
0
Perimeter (mm)
5
4
3
2
1
0
Circularity
1.0
0.8
0.6
0.4
Mfn1/2-/-
C
Mfn1/2 +/+
Mfn1/2 -/-

Fig.2

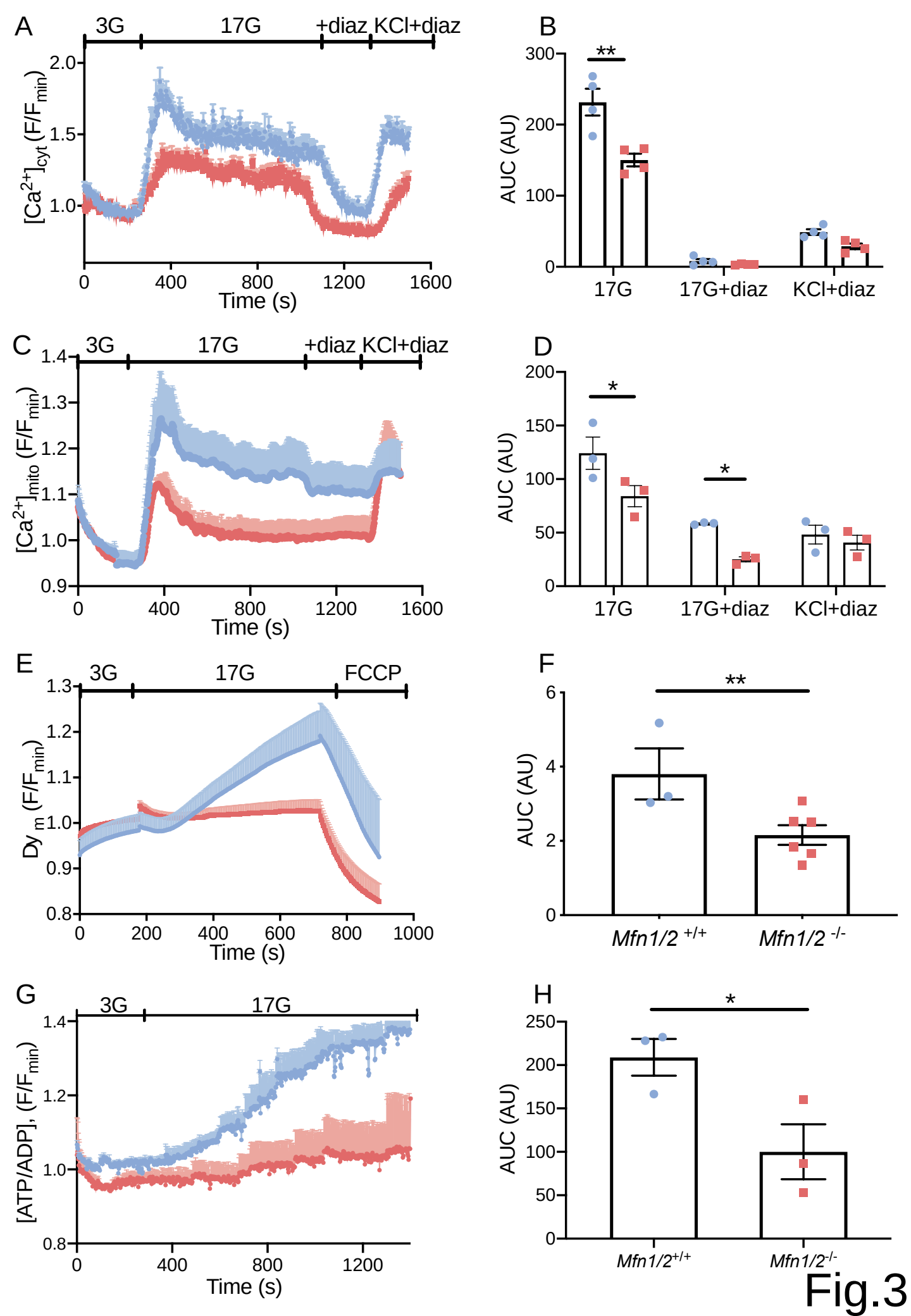
A
3G
17G
+diaz
KCl+diaz
[Ca2+]cyt (F/Fmin)
Time (s)
B
AUC (AU)
**
17G
17G+diaz
KCl+diaz
C
[Ca2+]mito (F/Fmin)
D
*
E
FCCP
Dy m (F/Fmin)
F
Mfn1/2 +/+
Mfn1/2 -/-
G
[ATP/ADP], (F/Fmin)
H
Mfn1/2+/+
Mfn1/2-/-
Fig.3

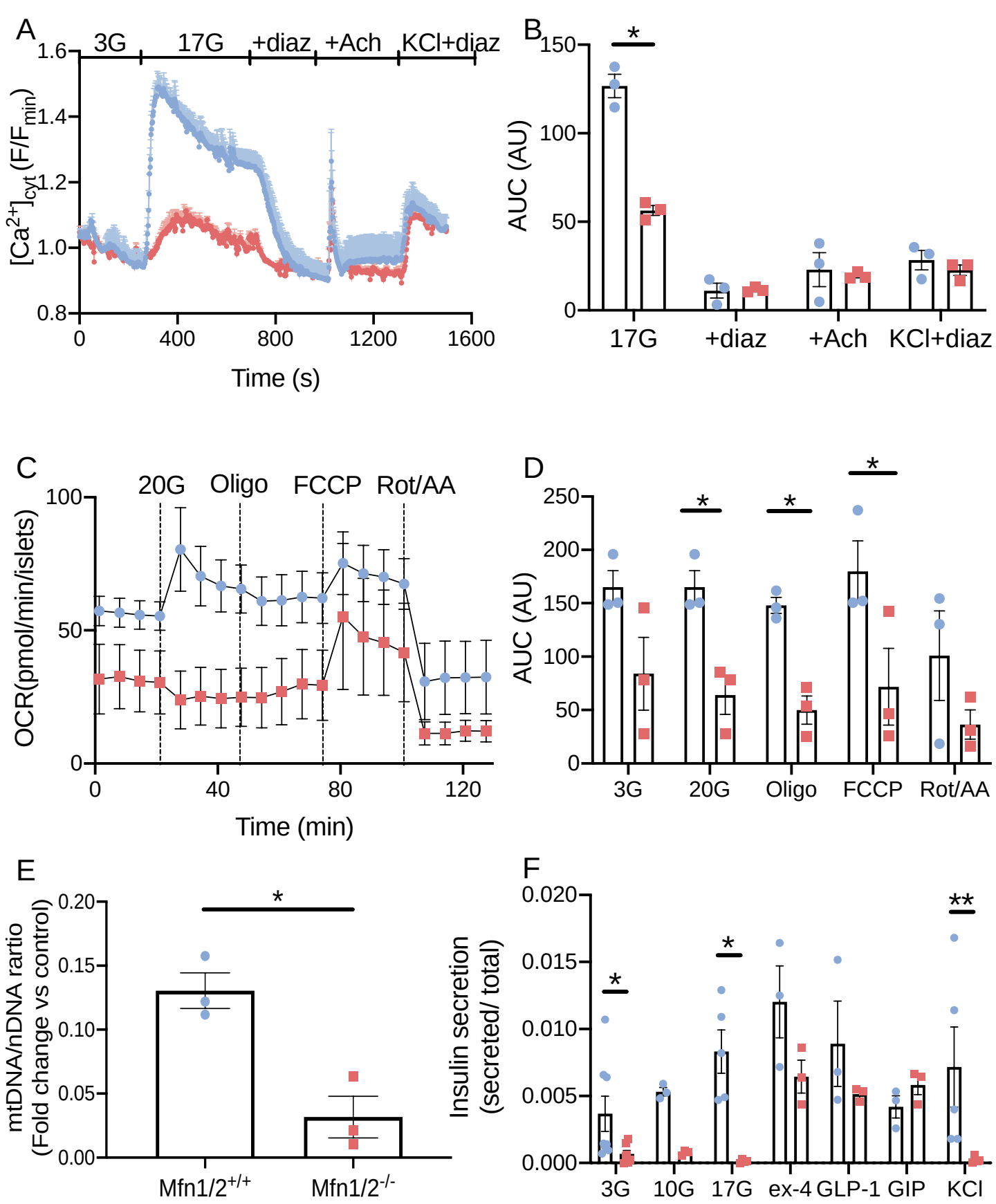
A
3G
17G
+diaz
+Ach
KCl+diaz
[Ca2+]cyt (F/Fmin)
Time (s)
B
AUC (AU)
17G
+diaz
+Ach
KCl+diaz
C
20G
Oligo
FCCP
Rot/AA
OCR(pmol/min/islets)
Time (min)
D
AUC (AU)
3G
20G
Oligo
FCCP
Rot/AA
E
mtDNA/nDNA rartio
(Fold change vs control)
Mfn1/2+/+
Mfn1/2-/-
F
Insulin secretion
(secreted/ total)
3G
10G
17G
ex-4
GLP-1
GIP
KCl

Fig.4

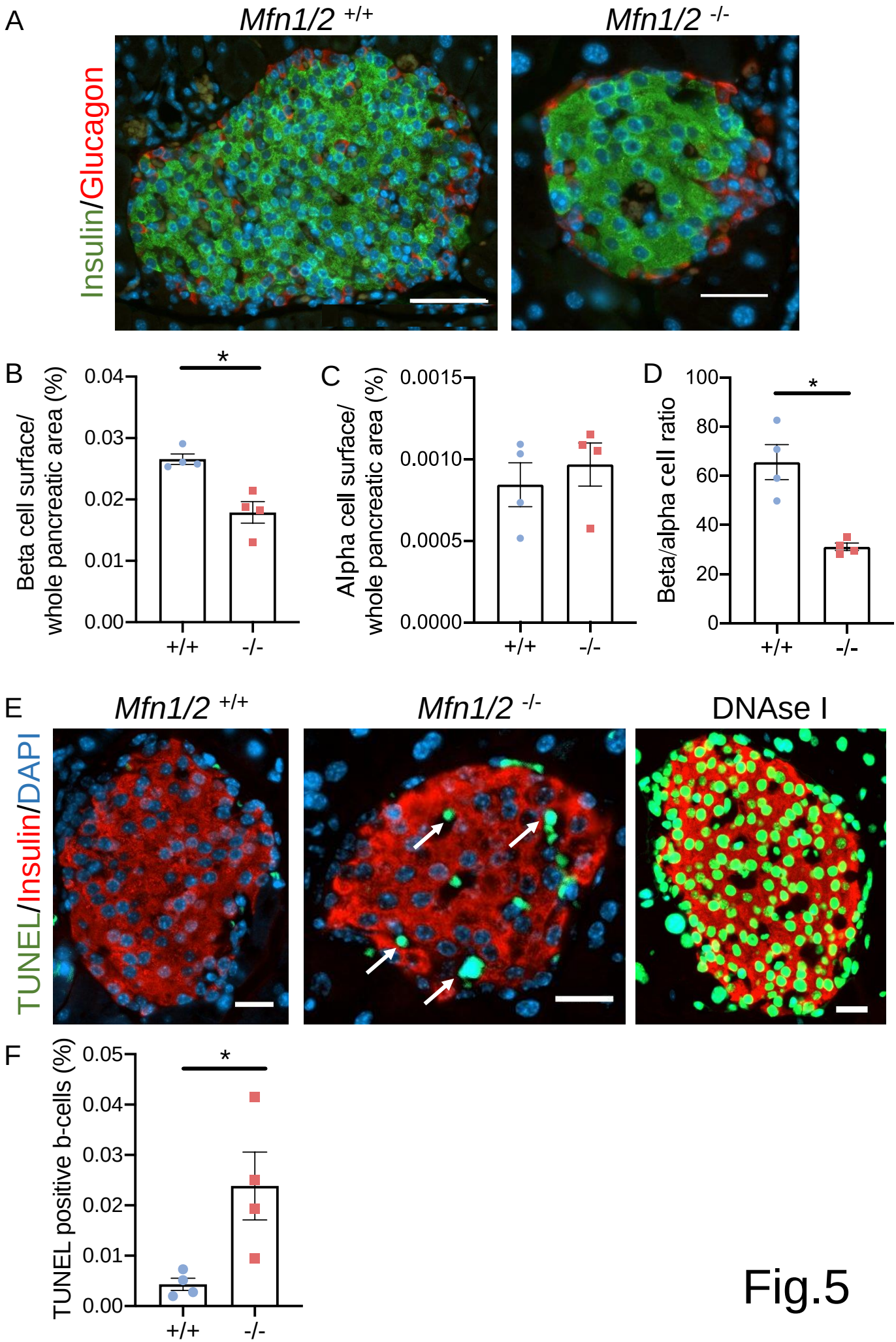
A
Mfn1/2 +/+
Mfn1/2 -/-
Insulin/Glucagon
B
Beta cell surface/ whole pancreatic area (%)
0.04
0.03
0.02
0.01
0.00
*
+/+
-/-
C
Alpha cell surface/ whole pancreatic area (%)
0.0015
0.0010
0.0005
0.0000
+/+
-/-
D
Beta/alpha cell ratio
100
80
60
40
20
0
*
+/+
-/-
E
Mfn1/2 +/+
Mfn1/2 -/-
DNAse I
TUNEL/Insulin/DAPI
F
TUNEL positive b-cells (%)
0.05
0.04
0.03
0.02
0.01
0.00
*
+/+
-/-

Fig.5

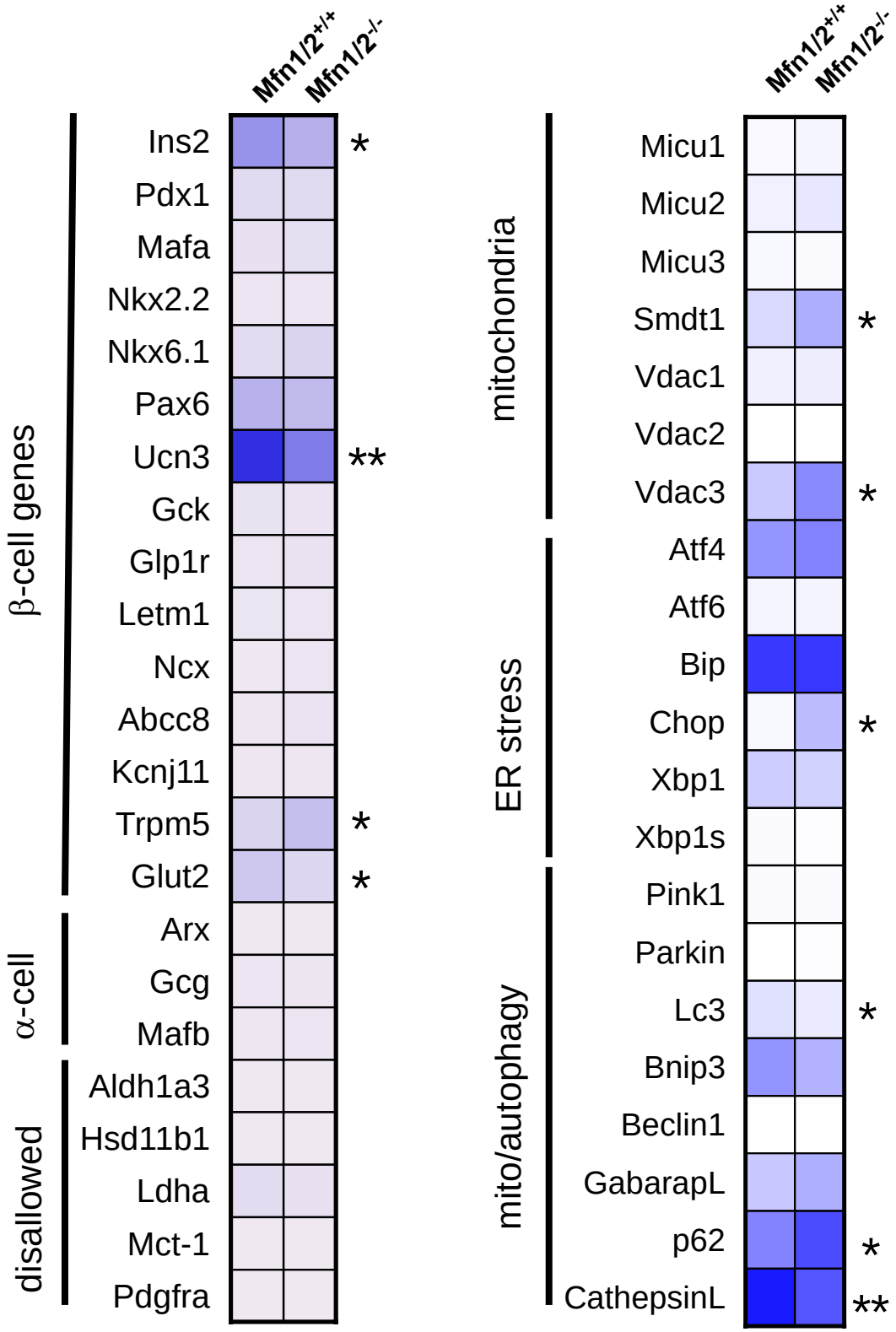
Mfn1/2+/+
Mfn1/2-/-
β-cell genes
Ins2
Pdx1
Mafa
Nkx2.2
Nkx6.1
Pax6
Ucn3
Gck
Glp1r
Letm1
Ncx
Abcc8
Kcnj11
Trpm5
Glut2
α-cell
Arx
Gcg
Mafb
disallowed
Aldh1a3
Hsd11b1
Ldha
Mct-1
Pdgfra
*
**
*
*
mitochondria
Micu1
Micu2
Micu3
Smdt1
Vdac1
Vdac2
Vdac3
ER stress
Atf4
Atf6
Bip
Chop
Xbp1
Xbp1s
mito/autophagy
Pink1
Parkin
Lc3
Bnip3
Beclin1
GabarapL
p62
CathepsinL
*
*
*
**

Fig.6

A

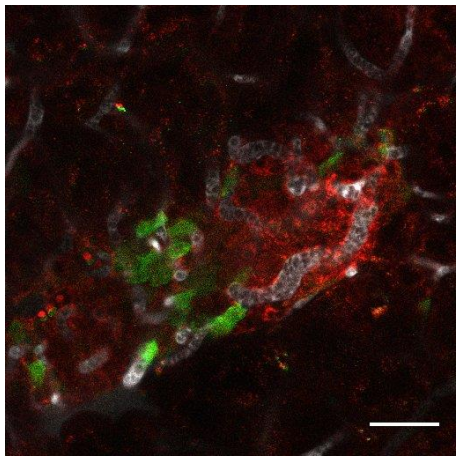
GCaMP6s/TMRM

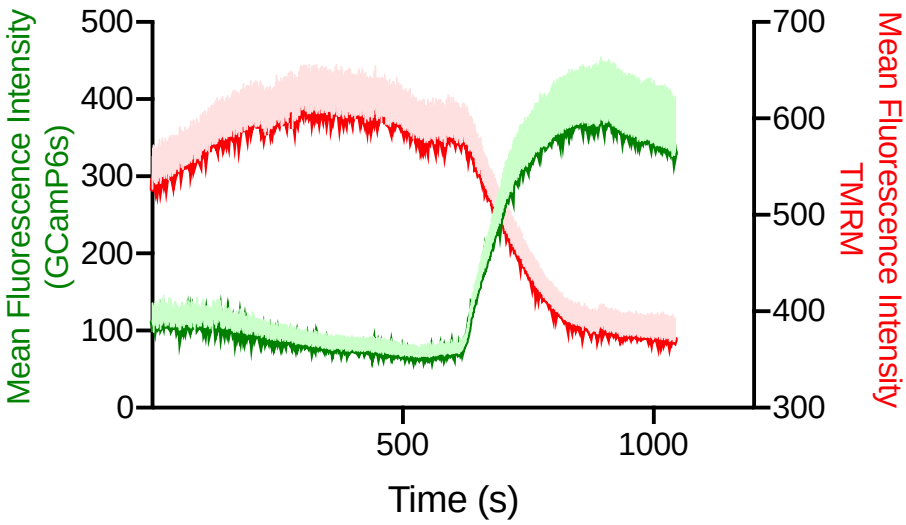
Mean Fluorescence Intensity (GCamP6s)
500
400
300
200
100
0
700
600
500
400
300
Mean Fluorescence Intensity TMRM
500
1000
Time (s)

B

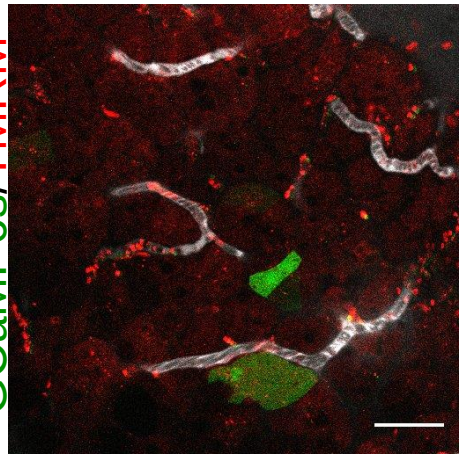
GCaMP6s/TMRM

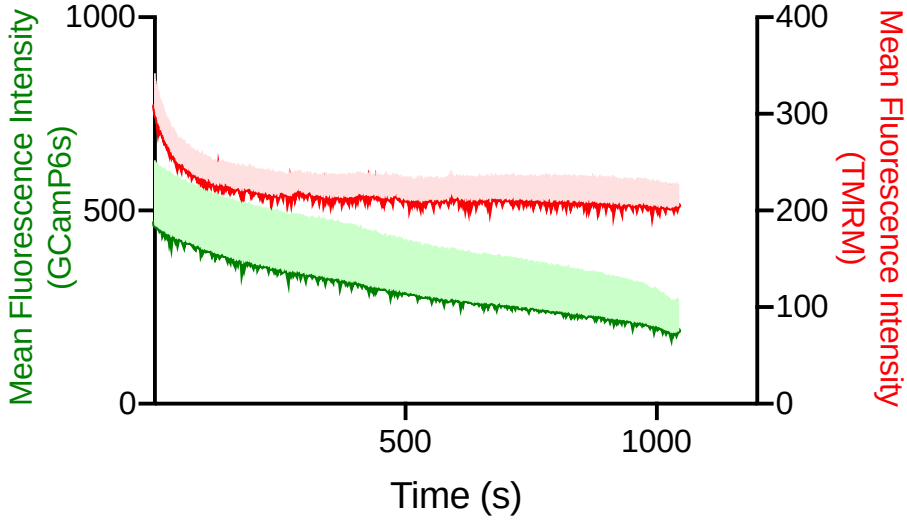
Mean Fluorescence Intensity (GCamP6s)
1000
500
0
400
300
200
100
0
Mean Fluorescence Intensity (TMRM)
500
1000
Time (s)

C

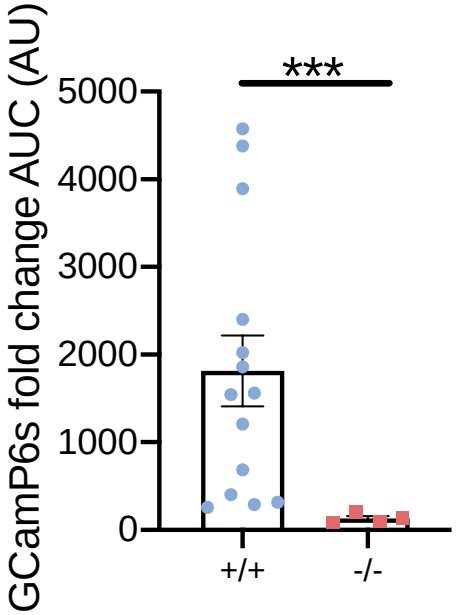
***
GCamP6s fold change AUC (AU)
5000
4000
3000
2000
1000
0
+/+
-/-

D

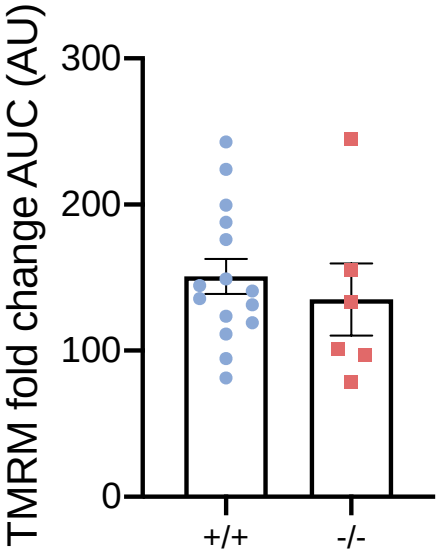
TMRM fold change AUC (AU)
300
200
100
0
+/+
-/-

Fig.7